ELSEVIER

Aerospace Science and Technology 6 (2002) 63–81

Aerospace Science and Technology

www.elsevier.com/locate/aescte

Modeling of sulfur gases and chemiions in aircraft engines

Modellierung von schwefelhaltigen Gasen und Chemi-Ionen in Flugzeug-Triebwerken

Alexander M. Starik [a], Alexander M. Savel'ev [a], Natalia S. Titova [a], Ulrich Schumann [b,*]

[a] *Central Institute of Aviation Motors, Scientific Research Center "Raduga", 111250 Moscow, Russia*

[b] *Deutsches Zentrum für Luft- und Raumfahrt (DLR), Institute of Atmospheric Physics, Oberpfaffenhofen, 82230 Wessling, Germany*

Received 17 August 2001; received in revised form 17 January 2002; accepted 17 January 2002

Abstract

The formation of sulfur-containing gases and chemiions in the combustor and their evolution in the turbine of aircraft-engines between combustor exit and engine exit are computed including the conversion fraction of fuel sulfur into SO_3 and H_2SO_4. The combustion is approximated by an adiabatic time-dependent box-model. The temperature and pressure evolution in the flow between combustor exit and engine exit is modeled using a quasi one-dimensional (Q1D) model. New kinetic models for S-containing gases and chemiions are used. About 1% of the sulfur molecules are computed to be converted into SO_3 within the combustor and about 10% into SO_3 and H_2SO_4 before engine exit. Box models agree with the Q1D results for the same initial and thermodynamic conditions, but underestimate sulfur conversion by a factor of 3 if using a linear temperature profile. The number of positive and negative ions formed within the combustor, mainly NO^+ and HSO_4^-, depends strongly on the fuel/air ratio and on recombination reactions, mainly with $C_2H_3O^+$ ions. The model computes a total ion emission of $2{\cdot}10^{15}$ per kg of fuel burned at cruise. Far larger ion concentrations close to values observed behind engines at ground, are computed for higher combustor inlet pressure and higher fuel/air ratio.

Zusammenfassung

Die Bildung von schwefelhaltigen Gasen und Chemi-Ionen in der Brennkammer von Flugzeugtriebwerken und ihre Veränderung in der Turbine zwischen Brennkammer und Treibwerksaustritt werden berechnet, einschließlich der Umwandlung von Treibstoff-Schwefel in SO_3 und H_2SO_4. Die Verbrennung wird mit einem adiabatischen instationären Box-Modell approximiert. Das Temperatur- und Druck-Profil entlang der Strömung vom Brennkammer-Austritt bis Triebwerks-Austritt werden mit einem quasi-eindimensionalen (Q1D) Strömungs-Model berechnet. Für die Kinetik der S-haltigen Gase und der Chemi-Ionen werden neue Modelle benutzt. Etwa 1% der Schwefelmoleküle werden in der Brennkammer in SO_3 und etwa 10% in der Turbine in SO_3 und H_2SO_4 umgewandelt. Für gleiche thermodynamische Bedingungen liefern Box-Modelle gleiche Ergebnisse, unterschätzen aber die Umwandlung um einen Faktor 3, wenn das Temperaturprofil in der Turbine durch ein lineares Profil approximiert wird. Die Zahl der positiven and negativen Ionen, die in der Brennkammer gebildet werden, vorwiegend NO^+ and HSO_4^-, hängt stark vom Treibstoff/Luft-Verhältnis und den Rekombinations-Reaktionen, vorwiegend mit $C_2H_3O^+$ Ionen, ab. Im Modell werden insgesamt $2{\cdot}10^{15}$ Ionen pro kg verbrannten Treibstoffs unter Reiseflugbedingengen emittiert. Sehr viel größere Konzentrationen, wie am Boden hinter Triebwerken gemessen, werden für höhere Brennkammerdrücke und Brennstoff/Luft-Verhältnisse berechnet.

Keywords: Combustion; Jet engine; Chemiion; Sulfur; Model

Schlüsselwörter: Verbrennung; Strahl-Triebwerk; Chemi-Ionen; Schwefel; Model

1. Introduction

Aerosols forming in the exhaust plume of aircraft engines may significantly perturb the chemical and physical

* Corresponding author.
E-mail address: ulrich.schumann@dlr.de (U. Schumann).

1270-9638/02/$ – see front matter
PII: S1270-9638(02)01150-1

processes in the atmosphere [7,27]. Most of the particles forming in exhaust plumes behind aircraft at cruise are liquid and contain sulfuric acid [13,45,50,53], and some condensable hydrocarbons [28,53]. The formation of volatile aerosols in aircraft plumes depends on the amounts of gaseous O, OH, SO_2, SO_3, and H_2SO_4, and on chemiions (CIs) emitted from the engines [22,61]. Sulfur dioxide is the main product of oxidation of fuel sulfur during burning of aviation kerosene in gas turbine engine combustors [8]. The concentrations of OH, SO_3, and H_2SO_4 at core engine exit depend on the non-equilibrium chemistry in the combustor and on reactions of the exhaust gases in the postcombustor flow from the combustor through the turbine and the expansion nozzle to the engine exit [9,36,46].

The fraction ε of conversion of SO_2 to SO_3 and H_2SO_4 is defined in terms of respective mole fractions as $\varepsilon = ([SO_3] + [H_2SO_4])/[SO_x]$, where SO_x includes all sulfur containing molecules resulting from fuel combustion. For homogeneous nucleation, the nucleation rate and the number density of volatile sulfate aerosol particles depends strongly on the magnitude of ε. If the volatile particles nucleate mainly on CIs, then ε controls the size of volatile particles formed [29].

The conversion fraction ε has been the topic of several studies [53]. Values of ε larger than 12–45% and 6–31% have been deduced from measurements of aerosols and CO_2 concentration behind a Concorde and a B-757 aircraft, respectively [18,38]. Direct measurements of sulfuric acid in the exhaust plume imply far smaller values of the sulfur conversion fraction ε of $\sim$1.2% [2], $>$0.4% [13], or 3.3% $\pm$1.8% [14]. Modeling studies assuming equilibrium conditions at combustor exit and taking into account the oxidation of SO_2 with OH and O radicals inside the engine between combustor and engine exit show that ε may reach values up to about 10% [8,36,46,58]. These calculations suffer from large uncertainties on the amount of SO_3, OH, O, and other gases formed within the combustor.

Another important precursor of volatile particles formed in aircraft engine exhaust are CIs [23,28,53,61,62]. Plume aerosol models require information on the type and concentration of ions reaching the nozzle exit. The ion formation inside an aircraft engine has not yet been modeled. Recent measurements in the exhaust of jet engines revealed negative ions with HSO_4^- cores, NO_3^- cores and ions containing C, H and O atoms [2,32] and positive ions including massive hydrocarbons [33]. The number density of ions at engine exit is still quite uncertain. For modeling nucleation consistent with volatile particle observations, engine exit CI number densities as large as 10^9 cm^{-3} have been assumed [61]. Such large CI concentrations were observed for a premixed rich acetylene-oxygen flame at a fuel/air equivalence ratio ϕ of 1.5–3 and an initial pressure of $\sim$20 torr [10,31] and in rich ($\phi = 2.13$) and lean ($\phi = 0.2$) premixed methane-oxygen flames at 40 torr [24] and 760 torr [43]. Maximum ion concentrations measured in such flames are $[H_3O^+] = 1.5{\cdot}10^{11}$ cm^{-3} and $[C_2H_3O^+] = 10^{10}$ cm^{-3}. But these flame conditions differ significantly from conditions in engine combustors which burn aviation kerosene with air under lean conditions ($\phi = 0.25$–0.33), at higher pressure $P_0 \approx 1$ MPa, higher temperature, and at shorter time scales (a few milliseconds). Moreover, the fuel/air ratio varies in a complex manner from rich to lean within the combustor. Only a few studies investigated the emission of CIs from aircraft engines. A total negative ion concentration of $1.4{\cdot}10^7$ cm^{-3} was measured at plume ages of about 10 ms after engine exit at ground [2]. Negative ions observed inside the plume of an Airbus A310 aircraft cruising at 10.4 km altitude at plume ages of about 2 s were found to be mainly $HSO_4^-(H_2SO_4)_m$, $HSO_4^-(HNO_3)_m$, and $NO_3^-(HNO_3)_m$ ions [3]. The upper limit concentrations of negative and positive ions estimated from the measurements was $3{\cdot}10^5$–$3{\cdot}10^6$ cm^{-3} for these conditions. Dilution [51] implies about 300 times larger concentrations at engine exit, and larger values to account for recombination processes. A total positive CI concentration of $1.6{\cdot}10^8$ cm^{-3} was measured in the exhaust of a jet engine at ground at 12 ms plume age [4]. The local number concentration c of ions per unit volume is related to an ion emission index EI (number of ions per unit mass of fuel burned) by $c = \mathrm{EI}\rho/N$, where ρ is the local plume gas density for given temperature and pressure, and N is the dilution factor (mass of air mixed with the exhaust from a unit mass of fuel burned [51]; for 16% hydrogen content in the fuel, the dilution factor in the engine is related to the equivalence fuel/air ratio ϕ by $N = 16.2/\phi$). Some models require an initial total ion concentration of the sum of positive and negative ions at engine exit of $4{\cdot}10^8$ cm^{-3} at temperature $T = 600$ K and pressure $P = 220$ hPa, or an ion emission index of $2{\cdot}10^{17}$ per kg of fuel burned [28,29,62]. For emission indices far larger than these values coagulation and recombination processes would quickly reduce the effective emission indices [61].

The dependence of ion emissions on the combustion process and the processes within the engine have not yet been determined. Therefore this paper investigates the formation of aerosol precursors in the combustor and the influence of various fluid dynamic and chemical kinetic processes within the gas turbine engine on the levels of sulfate aerosol precursors and CIs at engine exit.

2. Kinetic model

The formation of sulfur containing species (SO_x, HSO_3, H_2SO_4) and CIs within the combustor and in the engine, in the core flow from the combustor through the gas turbine and the nozzle, is simulated with a new kinetic scheme. The scheme involves more than 1000 reversible reactions with participation of 117 neutral gas species: H_z, N_z ($z = 1, 2$), O_x ($x = 1, \ldots, 3$), HO_x, H_2O_z, NO_x, HNO_y ($y = 1, \ldots, 4$), N_zH_y, C_z, C_mH_n ($m = 1, \ldots, 8$, $n = 1, \ldots, 18$), CO_z, HCN, $C_{m-1}H_{n-1}O_z$, S_z, SO_x, HSO_x, H_2SO_4, COS, H_2S, CS_2 and 35 negative (H^-, OH^-, O^-, O_2^-, O_3^-, O_4^-, CO_3^-, CO_4^-, CN^-, NO^-, NO_2^-, NO_3^-, SO_2^-, SO_3^-, SO_4^-, HSO_4^-) and

positive (CHO^+, CH_3^+, $C_2H_3^+$, $C_3H_3^+$, CH_2OH^+, $C_2H_3O^+$, C^+, CO^+, CO_2^+, H_3O^+, H_2O^+, O^+, O_2^+, N^+, N_2^+, NO^+, NO_2^+, NH_3^+, NH_4^+) ions. The kinetic model is based on our previous investigations of gaseous combustion kinetics for hydrocarbons-air mixtures [15,56,57]. The gas phase model for NO_x, HO_x and SO_x chemistry is close to a previously developed model [46]. The model was previously applied for an aircraft engine duct with prescribed initial conditions at combustor exit based on equilibrium calculations. The main reaction paths for NO_x, HNO_y, HO_x, SO_x, and HSO_y gases inside the mid-pressure turbine section were analyzed from that study. For the present study, the model has been extended to incorporate a more detailed S-containing species chemistry and a new ion-chemistry model. The reactions of SO_x-, S-, H_xS-, HSO_y- and CS_x-species included in the chemical model used in this paper are listed in the appendix, Table A1. All reactions are considered reversible. The rate constants of the backward reactions are determined from calculated equilibrium constants [46]. Large uncertainties exist in the sulfur chemistry, mainly because of missing data on reactions of SO_2 with OH at the high temperatures in the combustor and high pressure turbine [58]. The present study cannot contribute new information in this respect. For the formation of H_2SO_4 from SO_3 and H_2O [45] we note that the model uses a temperature independent summary reaction as suggested earlier [9,36].

The types of reactions for ion chemistry included in this kinetic model are listed in Table 1. The full set of ion reactions includes more than 400 reactions as listed in the appendix, Table A2. The block of ion chemistry is developed from measured ion kinetics during combustion [10, 11,17,41], shock waves in air [40], plasmochemical kinetics in electric discharge [35,42,55], and in the atmosphere [5,19–21,30,54]. Most of the rate constants for ion chemistry were determined only for low temperature ranges (300–500 K). For the far higher temperatures in the combustor and postcombustor flows, extrapolations are used in accordance with theory for the various types of reactions. For backward reactions for which the Arrhenius dependency is not listed in Table A2, the rate constants are determined using calculated equilibrium constants. The model does not include interactions with heavy hydrocarbon ions ($C_5H_3^+$, $C_7H_5^+$, $C_{13}H_9^+$, etc.) which are expected to be of small importance for lean engine combustion conditions. Many of the ion–ion and ion–neutral species reactions are known only with considerable uncertainty as discussed in the references cited. Nevertheless, the results computed with this kinetic scheme show a good correlation with experimental data on ignition delay in mixtures of hydrocarbons with air [56] and on CHO^+, $C_2H_3O^+$, H_3O^+, $C_3H_3^+$ ion concentrations in CH_4/air flames [41].

3. Chemiion formation during combustion

Aviation kerosene is a mixture of high-order hydrocarbons and contains 0.0001% to 0.3% sulfur per mass, with median values near 0.04%. Sulfur is contained in aromatic and polyaromatic groups of high-order hydrocarbons in the fuel. The fuel/air mixture enters the combustor of a mod-

Table 1
Reactions mechanism for chemiions formation

Type of reaction	Symbols	Reaction products
1. Reaction with CH, CH($a^4\Sigma^-$)	$CH(CH^*) + O = HCO^+ + e^-$ $CH^* + C_2H_2 = C_3H_3^+ + e^-$	HCO^+, $C_3H_3^+$, e^-
2. Associative ionization	$A + B = AB^+ + e^-$	N_2^+, O_2^+, NO^+, $C_3H_3^+$, e^-
3. Dissociative ionization	$AB + e^- = A^- + B$	O^-, O_2^-, NO_2^-
4. Ionization under molecule and electron interaction	$AB + e^- = AB^+ + 2e^-$	O_2^+, N_2^+, NO^+, O^+, N^+
5. Associative electron attachment	$AB + e^- = AB^-$	O^-, O_2^-, NO^-, NO_2^-
6. Nonresonance charge exchange	$A^+ + B = A + B^+$	N_2^+, N^+, O_2^+, O^+, NO^+, NO_2^+, NH_3^+, CO^+, CO_2^+
	$A^- + B = A + B^-$	NO_2^-, NO_3^-, O^-, O_2^-, O_3^-, H^-, OH^-, SO_2^-
7. Binary ion–molecular reactions	$A^+ + BC = B + AC^+$	HCO^+, H_3O^+, CH_2OH^+, H_2O^+, CH_3^+, $C_2H_3O^+$, $C_2H_3^+$, $C_3H_3^+$, C^+, N_2^+, N^+, NO^+, NO_2^+, NH_3^+, NH_4^+, O^+, O_2^+, CO^+
	$A^- + BC = B + AC^-$	NO^-, NO_2^-, NO_3^-, O^-, O_2^-, O_3^-, O_4^-, OH^-, CN^-, CO_3^-, CO_4^-, SO_2^-, SO_3^-, SO_4^-, HSO_4^-
8. Ion-molecular reactions with electron formation	$AB^- + C = e^- + A + BC$	e^-
9. Ternary recombination of ion and neutral	$A^+ + B + M = AB^+ + M$	N_2^+, NO^+, O_2^+
10. Dissociative recombination	$A^- + B + M = AB^- + M$	NO_2^-, O_3^-, CO_3^-, O_4^-, O^-, CO_4^-
	$AB^+ + e^- = A + B$	Neutral
11. Ion–electron recombination	$AB^+ + e^- = AB$	Neutral
12. Binary ion-ion recombination	$AB^- + C^+ = AB + C$	Neutral
13. Ternary ion-ion recombination	$AB^- + C^+ + M = AB + C + M$	Neutral

ern gas turbine engine typically with initial temperature $T_0 = 1000$ K and pressure $P_0 = 1$ MPa. After thermal destruction of these hydrocarbons in the combustor, lighter hydrocarbons form and the sulfur contained in the hydrocarbon fuel is transformed into H_2S. Our model assumes an initial mixture containing n-C_8H_{18} thermal destruction products (16% hydrogen mass fraction) mixed with air and H_2S at an equivalence fuel/air ratio $\phi = 0.25$ (dilution factor $N = 64.7$).

The ignition and combustion process in the combustor is simulated by integrating the kinetic equations versus time assuming a homogenous mixture in an adiabatically closed reactor from a time before ignition until an exit time τ_{exit}. The value of τ_{exit} is selected such that the computed emission index of NO_x is in agreement with the NO_x emission index of an *RB211* engine of type *RB211-524B* measured on an altitude test chamber [49]. We use $\tau_{\text{exit}} = 1$ s for cruise conditions with $T_0 = 1000$ K, $P_0 = 1$ MPa, $\phi = 0.25$, and $\tau_{\text{exit}} = 10^{-2}$ s for ground conditions with $T_0 = 1250$ K, $P_0 = 4.5$ MPa, $\phi = 0.33$ or 0.25. For cruise conditions, Fig. 1 depicts the temporal evolution of the computed mixing ratios of N- (a), and S-containing (b) species, and CIs (c) during combustion of C_8H_{18} thermal destruction products mixed with air and H_2S for a typical fuel sulfur content (FSC) of 0.04%. Ignition occurs at $t \sim 10^{-2}$ s. After ignition the combustion products contain relatively large amounts of SO_2, some SO_3, and smaller amounts of HSO_3 and H_2SO_4, and trace amounts of $C_2H_3O^+$, NO^+, H_3O^+, HSO_4^-, SO_3^-, and NO_3^- ions. Some species such as HSO and SO_3^- get formed temporarily during ignition and disappear when the reactions continue for more than 0.1 s in the closed reactor in these simulations. The gas species SO_3, HSO_3, H_2SO_4, NO, NO_2, NO_3, HNO_2, HNO_3, OH, HO_2, O, and the CIs at the combustor exit do not reach local chemical equilibrium. The S-containing species concentrations reach their equilibrium values at significantly shorter time scales than the N-containing species and the CIs. The value of τ_{exit} selected to match observed NO_x emission values is rather large and not realistic. Also the combustor inlet temperature selected is higher than in typical engine combustors. This reflects the difficulty in simulating the complex combustion process with a well-mixed reactor. The model succeeds in describing the self-ignition process and is used for some first parameter studies, but more refined model studies are to be performed in the future to simulate the combustion process in more detail.

The amounts of sulfur containing gases and of ions HSO_4^-, SO_3^-, and NO_3^- depend on the fuel sulfur content. The model results for neutral species and ion mole fractions for two values of FSC are listed in Table 2. The amount of O leaving the combustor is only 6% of the amount of OH radicals, which agrees roughly with equilibrium estimates and implies that the oxidation of SO_2 to SO_3 with O is of minor importance compared to reactions with OH [58]. The computed NO_x emission index is 18 g/kg which fits the AERONOX data for the *RB211* engine [49] because of

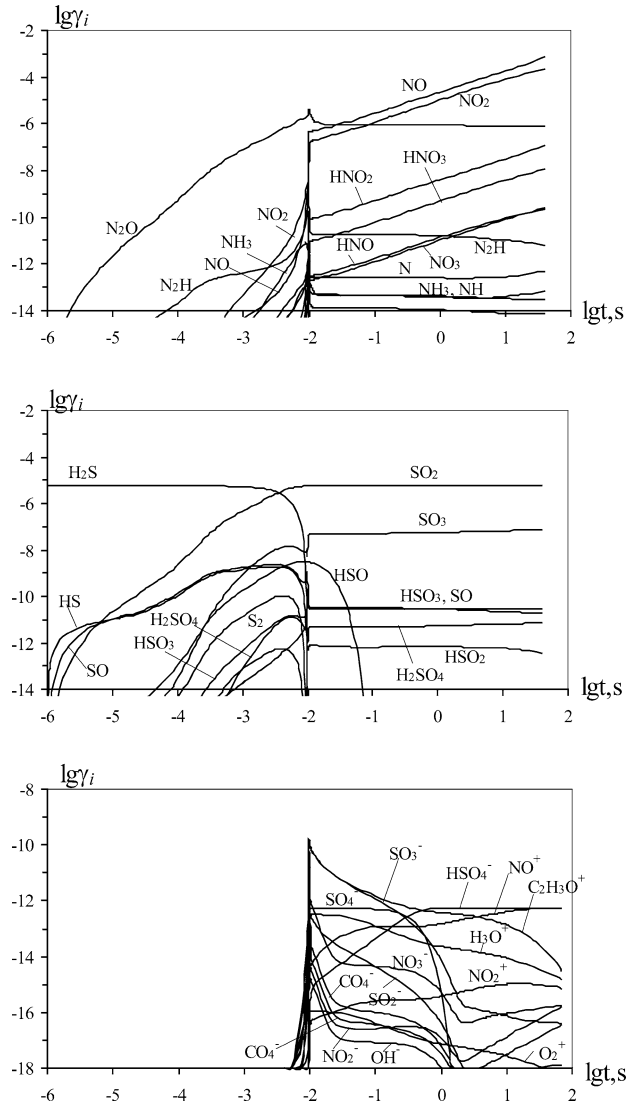

Fig. 1. Evolution of N- and S-containing gas species and ions mole fractions versus time of combustion for C_8H_{18} destruction products mixed with air and H_2S, at fuel/air ratio $\phi = 0.25$, temperature $T_0 = 1000$ K, pressure $P_0 = 1$ MPa, and fuel sulfur content $FSC = 0.04\%$.

the selected τ_{exit} value. The $[NO_2]/[NO_x]$ ratio is close to 0.3 and fairly insensitive to the value of τ_{exit} (see Fig. 1a). The ratio is larger than what was measured for the *RB211*, possibly because of inadequacy of the simple model, but close to what was found for a smaller engine (*PW305*) in the AERONOX project, and is not unrealistic when compared to measurements in the exhaust plume behind cruising aircraft [48,52,59].

The concentrations of positive and negative ions (and of most gas species) strongly depend on the fuel/air equivalence ratio ϕ. Note that ϕ varies locally within the combustor because of inhomogeneous fuel air mixing and other features of combustion, whereas this study assumes a homogeneous mixture. The temporal evolution of positive and negative ion concentrations versus time is shown in Fig. 2 for $\phi = 0.5$, 0.33, and 0.25. The time required for approach-

Table 2
Neutral gas species and ion mole fractions under combustion of thermal destruction products of the mixture of C_8H_{18} with air and H_2S at $\phi = 0.25$, $P_0 = 1$ MPa, for two values of fuel sulfur content (*FSC*) of 0.04% and 0.3%, and for ignition time τ_{in} and exit time τ_{exit} from the combustor

Species	τ_{in}		τ_{exit}	
	FSC, %		FSC, %	
	0.04	0.30	0.04	0.30
O	2.90(−4)	2.83(−4)	8.47(−6)	8.43(−6)
O_2	1.60(−1)	1.61(−1)	1.54(−1)	1.54(−1)
O_3	2.78(−7)	2.77(−7)	4.30(−9)	4.29(−9)
H	2.25(−5)	2.21(−5)	5.27(−8)	5.25(−8)
H_2	5.27(−5)	5.38(−5)	5.25(−7)	5.23(−7)
OH	4.81(−4)	4.67(−4)	1.40(−4)	1.40(−4)
HO_2	4.18(−6)	4.27(−6)	1.02(−6)	1.02(−6)
H_2O	3.93(−2)	3.93(−2)	3.99(−2)	3.99(−2)
N	2.36(−12)	2.34(−12)	2.59(−13)	2.56(−13)
N_2	7.68(−1)	7.68(−1)	7.74(−1)	7.74(−1)
NO	4.85(−8)	4.58(−8)	1.15(−4)	1.14(−4)
NO_2	1.84(−9)	1.80(−9)	5.43(−5)	5.39(−5)
NO_3	3.03(−15)	2.92(−15)	5.18(−11)	5.14(−11)
HNO	4.24(−12)	4.04(−12)	6.16(−11)	6.10(−11)
HNO_2	7.06(−11)	6.71(−11)	1.97(−8)	1.95(−8)
HNO_3	1.41(−12)	1.39(−12)	2.57(−9)	2.55(−9)
N_2O	2.70(−6)	2.67(−6)	7.94(−7)	7.92(−7)
NH_3	7.54(−13)	7.53(−13)	3.44(−14)	3.42(−14)
CO	1.46(−2)	1.49(−2)	1.19(−6)	1.19(−6)
CO_2	1.65(−2)	1.62(−2)	3.15(−2)	3.14(−2)
SO	1.11(−9)	8.30(−9)	2.34(−11)	1.75(−10)
SO_2	5.67(−6)	4.26(−5)	5.66(−6)	4.25(−5)
SO_3	6.47(−9)	4.96(−8)	6.49(−8)	4.88(−7)
HSO_3	2.07(−10)	1.54(−9)	2.74(−11)	2.05(−10)
H_2SO_4	1.08(−12)	8.36(−12)	6.22(−12)	4.69(−11)
H_3O^+	1.08(−13)	9.82(−14)	1.14(−14)	1.61(−14)
NO^+	4.63(−17)	3.88(−17)	3.33(−13)	4.65(−13)
NO_2^+	8.13(−20)	6.77(−20)	8.92(−16)	1.25(−15)
$C_2H_3O^+$	1.19(−10)	1.12(−10)	1.95(−13)	2.91(−13)
NO_2^-	2.49(−13)	1.00(−13)	6.99(−18)	1.26(−18)
NO_3^-	6.60(−14)	2.62(−14)	7.34(−17)	1.35(−17)
SO_2^-	1.29(−13)	3.98(−13)	1.71(−18)	1.60(−18)
SO_3^-	2.47(−11)	7.58(−11)	9.63(−17)	1.03(−16)
SO_4^-	1.19(−13)	3.66(−13)	4.50(−20)	5.55(−20)
HSO_4^-	7.53(−19)	1.72(−18)	5.40(−13)	7.73(−13)
CO_3^-	7.19(−11)	2.73(−11)	4.37(−19)	6.44(−20)
CO_4^-	2.18(−11)	8.35(−12)	5.03(−19)	9.00(−20)

A(n) corresponds $A \cdot 10^n$.

ing local chemical equilibrium is longer and the CI concentrations (both their maximum values after ignition and their equilibrium ones) are lower for lower values of ϕ. At $\phi = 0.5$, the maximum values of the HSO_4^- and NO^+ mixing ratios are around $4 \cdot 10^{-10}$ and the $C_2H_3O^+$, H_3O^+, SO_3^-, and NO_3^- mixing ratios are larger than 10^{-8}. At $\phi = 0.25$, HSO_4^- reaches a mixing ratio of $5.5 \cdot 10^{-13}$. Hence inhomogeneous mixing, with larger local fuel/air ratio, may also cause larger CI concentrations. The strong dependence of ion concentration from the ϕ value is a consequence of larger temperature and larger concentration of CH radicals after ignition for larger ϕ values ($\phi < 1$). Higher temperature and larger CH concentrations result in larger rates of CHO^+ ions and electrons formation. An increase of ϕ from 0.25 to 0.5 in the model increases the mixing ratio of CHO^+ and e^- after ignition by nearly a factor of $\sim 10^4$. An increase of ϕ also causes a larger O/OH concentration ratio (the O/OH equilibrium ratio is $\sim 0.05, 0.1, 0.2$, for $\phi = 0.25, 0.33, 0.5$, respectively).

The major reaction paths of ion formation under combustion of S-containing hydrocarbon fuel/air mixtures in our model are identified in Fig. 3. In a first step CHO^+ ions and electrons form by reactions of CH radicals in ground electronic state and excited radical $CH^*(a^4\Sigma)$ with O atoms:

$$CH + O = CHO^+ + e^-,$$
$$CH^*(a^4\Sigma) + O = CHO^+ + e^-.$$

The primary negative ions O_2^- quickly form by associative ionization reactions of electrons and O_2 molecules. The O_2^- ions react with CO_2 and O_2 to form CO_4^- and O_4^- ions.

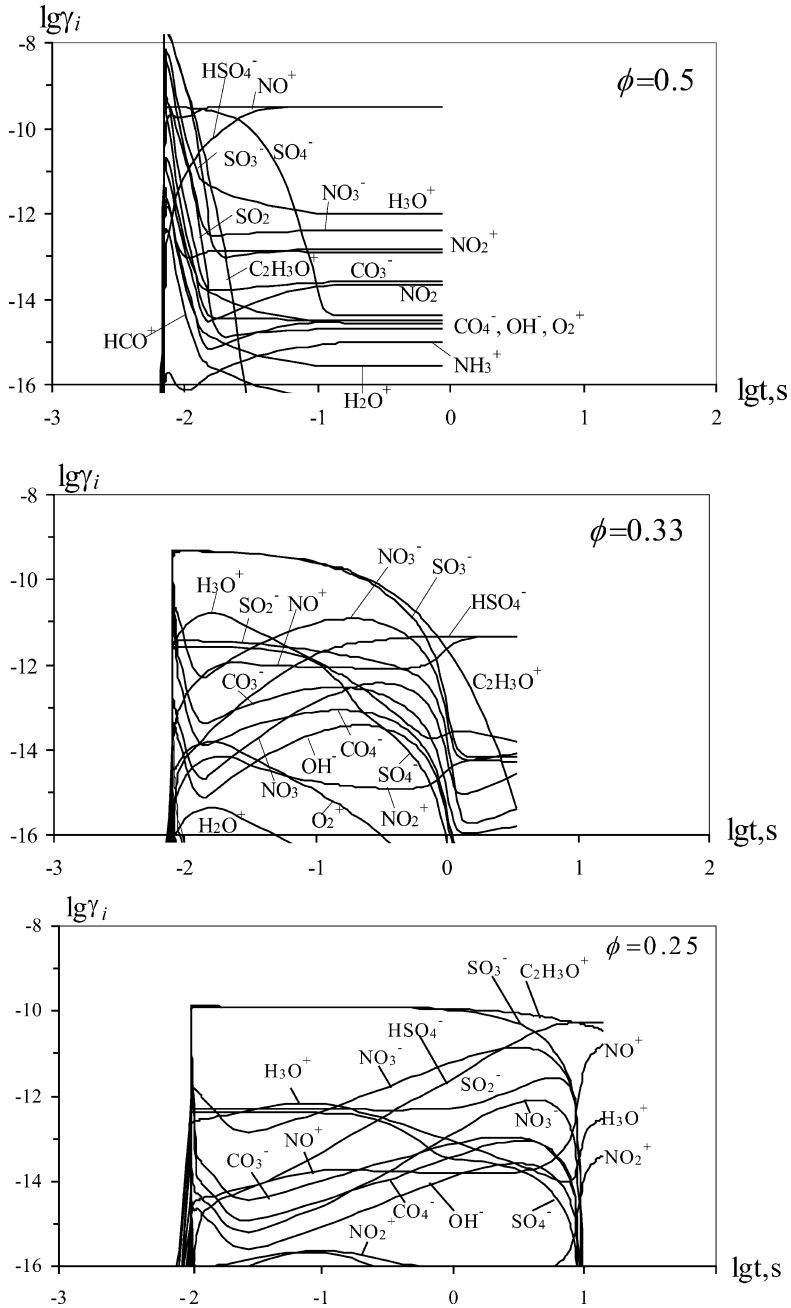

Fig. 2. Evolution of chemiion mole fractions versus time of combustion of C_8H_{18} destruction products mixed with air and H_2S at $T_0 = 1000$ K, $P_0 = 1$ MPa, $FSC = 0.04\%$ and various values of fuel/air equivalence ratio, $\phi = 0.5$, 0.33, and 0.25.

Reactions of O_4^- ions with CO molecules and of CO_4^- ions with O atoms result in the formation of CO_3 and O_3^- ions. Coincidentally with these processes, the HCO^+ ions react with H_2O molecules and CH_2 radicals and this results in the rise of H_3O^+ and CH_3^+ ions. The H_3O^+ and CH_3^+ ions react with C_2H_2 and H_2 molecules giving rise to $C_3H_3^+$ and $C_2H_3O^+$ ions at later times. Reactions of CO_3^- ions with O atoms and SO_2 molecules produce O_2^- and SO_3^- ions. Reactions of CO_4^- ions with SO_2 and NO molecules lead to formation of SO_4^- and NO_2^- ions. These ions are responsible in this model for the generation of negative ions SO_2^-, HSO_4^-, and NO_3^-. The positive ions H_2O^+, O_2^+, NO_2^+, and NO^+ form from reactions with H_3O^+ and H_2O^+ ions. For negative ions, a similar reaction path scheme has been suggested which includes also the formation of ion clusters $HSO_4^- HNO_3$ and $HSO_4^- H_2SO_4$ in the exhaust plume outside the engine [23].

Our model computes maximum ion concentrations which may appear small compared to laboratory measurements [10]. Our modeling studies reveal that ion concentrations during combustion decrease mainly by recombination reactions with $C_2H_3O^+$:

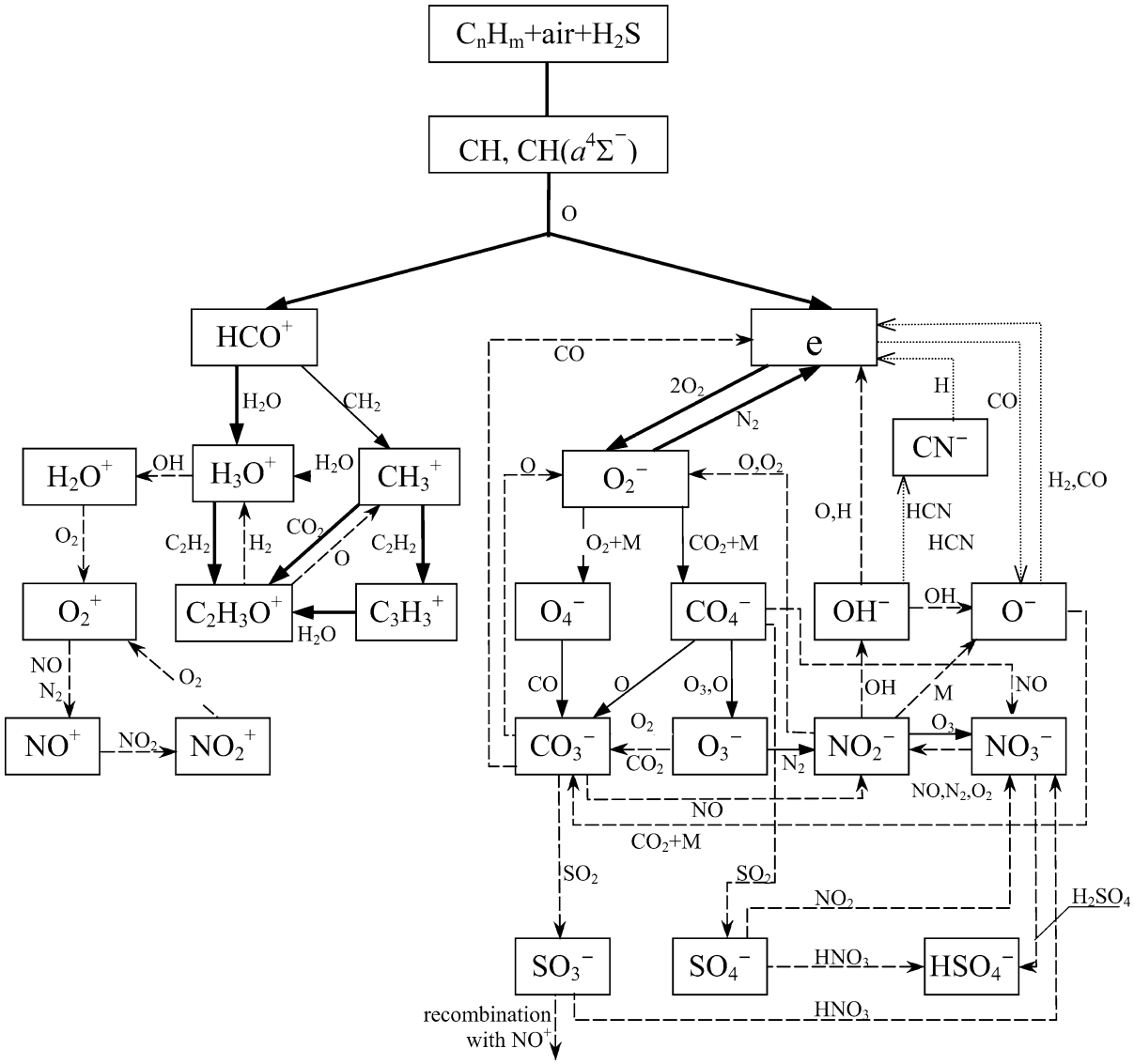

Fig. 3. Scheme of chemiion formation paths under combustion of S-containing hydrocarbon fuels with air. In this scheme solid lines depict the processes of ion formation during ignition time (thick lines correspond to more rapid reactions, and thin lines correspond to slower reactions). Long dashed lines depict the processes of ion formation after ignition time, when the temperature and ion concentration is relatively high. Short dashed lines depict the processes occuring in rich flames ($\phi > 1$).

$$SO_3^- + C_2H_3O^+ = SO_3 + C_2H_3O,$$
$$NO_3^- + C_2H_3O^+ = NO_3 + C_2H_3O.$$

In order to determine an upper limit of ion concentrations in the combustor for the given kinetic reaction scheme, a modified kinetic model is used in which these most important recombination reactions are excluded. In this case, at $\phi = 0.25$, the most abundant ions are HSO_4^- and $C_2H_3O^+$ which reach concentrations of $3.9{\cdot}10^9$ cm^{-3}. The values of ion number density at combustor exit, for $\phi = 0.25$ and $FSC = 0.3\%$, for the two kinetic models, with and without the recombination reactions with $C_2H_3O^+$ differ by a factor of 100, implying an upper limit of ion number density of $4{\cdot}10^9$ cm^{-3}. The ion number density computed with all recombination reactions should be the more realistic one and amounts to $\sim 4{\cdot}10^7$ cm^{-3}. Far larger ion concentrations ($>10^{10}$ cm^{-3}) were measured for CH_4/O_2 flames at $\phi = 1$ and 0.5 [10]. However for combustion of aviation kerosene with air in lean flames with $\phi = 0.25$ the values of ion number density should be significantly smaller, because of the lower combustion temperature. We cannot exclude, however, that other CI source reactions occur which are not included in our model. Differences between our model results and measurements may also result from approximating kerosene by the thermal destruction products of n-C_8H_{18} with air. In real combustors the combustion of kerosene may lead to another rate of CH radical formation and result in different CHO^+ and other ions concentrations. Finally, our model does not account for interactions of the gaseous species and ions with soot.

4. Composition of gases and chemiions in the engine

4.1. Model for calculation of parameters in the postcombustor flow

Two models were used to investigate the production of sulfate aerosol precursors and CIs in the flow between combustor and engine exit. The two models differ essentially in the treatment of the flow inside the turbine. The Q1D model [46] treats the temperature, pressure, velocity and gas composition according to the one-dimensional conservation principles along the flow through the turbine, including blade effects. The second model is a box model in which temperature and pressure is prescribed as a function of time [58]. In this box model study, it was assumed that the temperature decreases linearly from combustor exit to nozzle exit and that the pressure decreases faster according to a prescribed hyperbolic function of time along the flow. We study the change in gas and ion concentrations along the engine duct and the implications of such box model simplifications for conditions approximating the core of engines of type *RB211* and *JT9D-7A*, as used for *B-757* and *B-747* subsonic aircraft. The same engines have been considered in previous modeling and experimental studies [46,58]. The boundary conditions (T, P and gas composition) at combustor exit for these calculations are taken from the combustion calculations for $\phi = 0.25$; $T_0 = 1000$ K; $P_0 = 1$ MPa described in the previous section (Table 2).

Fig. 4 depicts the evolution of temperature T_r and pressure P_r with time after exit from the combustor as computed with the Q1D model (full curve) inside the turbine for the *RB211* engine under cruise condition of a *B-747* aircraft (altitude $H = 10.7$ km, Mach number $M_0 = 0.8$). The linear temperature approximation, represented by the dashed line, deviates considerably from the Q1D result. Fig. 5 depicts the evolution of the H-, N-, and S-containing gas species concentrations computed with the Q1D model inside the engine for two different FSC values.

The values of mole fractions γ_i of neutral species and CIs, temperature, and pressure during the postcombustor flow versus time t at characteristic cross sections of the internal flow are listed in Table 3 for $FSC = 0.3\%$. The temperature decreases from 1540 K at combustor exit to 598 K at nozzle exit. The mole fractions γ_i vary considerably for most of the components with minor variations only for H_2O, O_2, N_2, and CO_2. The variations of the γ_i values are most pronounced for strong oxidizers such as O, OH, and HO_2, as well as for NO_3 and for members of the N_xH_y group. The effective mass emission index of OH amounts to 5.4 g/kg at combustor exit and 66 mg/kg at engine exit. At engine exit, most of the initially formed OH radicals are depleted by reactions with NO, NO_2, SO_2 and others, leaving a mole fraction of about 10^{-6}, and this explains why measurements so far found hardly significant traces of OH at engine exit [6]. From measurements of HNO_2, HNO_3, NO, and NO_2 in aged exhaust plumes, OH emission indices of 60 to 400 mg/kg have been derived using models describing the chemistry in the diluting plume, starting from engine exit [52,59]. This fits reasonably with the present model results. The small amount of OH emitted from the engine exit implies small (< 1%) additional sulfur conversion to H_2SO_4 after engine exit [59]. It should be noted that the concentrations of HNO_2 and HNO_3 in the turbine affect each other (Fig. 5; see [46]). The local maximum in HNO_3 near $t = 1.8$ ms is caused by a change in importance of various reactions at this time. At early stage of expansion in the turbine ($t \leqslant 1.8$ ms), the increase in HNO_3 is caused mainly by the reactions $NO_2 + OH + M = HNO_3 + M$ and $O_2 + HNO_2 = O + HNO_3$. After $t = 1.8$ ms, the decrease

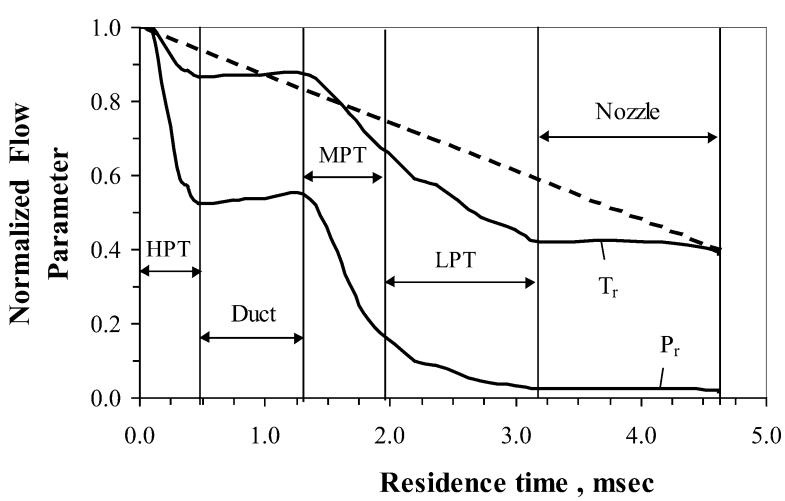

Fig. 4. Temperature and pressure evolution in the flow from the combustor exit to engine exit within an *RB211* core engine at cruise conditions of a *B-747* aircraft. Solid lines correspond to temperature T and pressure P as obtained by simulation of the postcombustor flow using the Q1D model, and the dotted line depicts a linear variation of T with time. The values are normalized by the initial values. Arrows indicate the ranges of the high-pressure turbine (HPT), the duct between high- and medium-pressure turbines, the medium-pressure turbine (MPT), the three-stage low-pressure turbine (LPT), and the exhaust nozzle until nozzle exit.

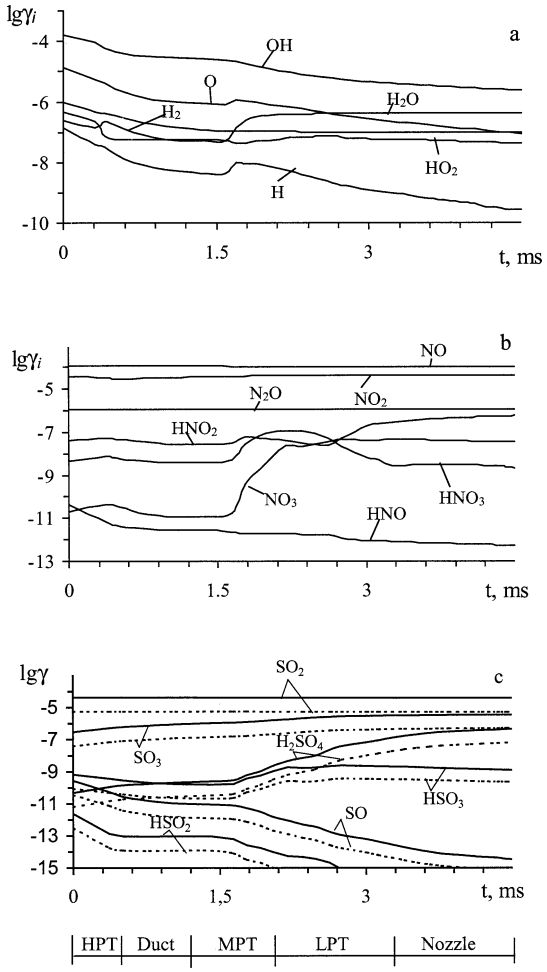

Fig. 5. H- (a), N- (b), and S-containing (c) gas species mole fractions in the postcombustor flow of a *RB211* engine at $FSC = 0.04\%$ (dashed curves) and $FSC = 0.3\%$ (solid curves).

of HNO_3 concentration and the formation of NO_3 is caused mainly by the reactions $HNO_3 + OH = NO_3 + H_2O$ and $HNO_3 + M = H + NO_3 + M$.

Significant SO_2 oxidation occurs throughout the turbine resulting in up to 9% oxidation of the total SO_x to (SO_3+H_2SO_4) at engine exit for $FSC = 0.04\%$, and 8.4% conversion for $FSC = 0.3\%$. The NO_3 and HNO_2 concentrations also increase significantly within the postcombustor flow but stay below 1% of the sum of NO and NO_2 species, as found in measurements [1,52,58].

At nozzle exit, NO^+ and HSO_4^- ions are the most abundant ones. The presence of HSO_4^- ions is consistent with recent mass spectrometric measurements after engine exit [32,33]. However, NO^+ ions were not observed within these measurements. These measurements identified only ions with masses larger than 50 atomic mass units. It is well known that NO^+ ions may be generated in large amounts in shock waves in air [34,40]. NO^+ ions were also observed in H_2/air flames [25] and in acetylene and propane/air flames [22]. The model does not take into account the formation of $NO^+(H_2O)_n$ clusters and their possible reactions with molecules possessing proton affinities larger than that of H_2O [33]. Ions $NO^+(H_2O)_n$ are presumably unstable at the high temperatures inside the engine but may form in the cool exhaust plume outside the engine.

The mole fractions of the major ions and the sum of all ions does not vary much along the duct in the model (see Table 3). Instead, the total ion concentration is controlled mainly by the amount of ions formed in the combustion chamber, because the recombination time is much larger than the transit time within the postcombustor duct for the given concentrations. For larger initial ion concentrations at combustor exit, ion–ion-recombination reactions in the turbine would be more important. As it was mentioned above, the computed ion concentration at combustor exit strongly depends on the treatment of recombination reactions with $C_2H_3O^+$ in the kinetic model. The recombination reactions inside the combustor reduce the ion concentrations at nozzle exit by a factor of order of 100. Without these recombinations, the ion concentration sum would reach an upper limit of $4.3{\cdot}10^8$ cm^{-3}, corresponding to an emission factor of $2.3{\cdot}10^{17}$ kg^{-1}. However the recombination reactions do occur and hence the sum of the ion concentration (maximum for HSO_4^-) amounts to only about $4.5{\cdot}10^6$ cm^{-3} at nozzle exit at cruise or an ion emission index of $2{\cdot}10^{15}$ kg^{-1} in our model. This is less than expected from measurements at the ground [2,4] and less than required to explain the number of volatile particles formed with models [29].

The larger observed ion concentration at ground may be explained partly by different engine operation conditions at ground compared to cruise altitude. Another possible reason results from local variations in the fuel/air ratio within real combustors. The details of the flow inside the combustor are very complicated and not represented in our model. Variations in the fuel/air ratios within the combustor ($\phi = 1/0.2$) could cause locally higher temperature and larger ion concentration. The temperature and pressure at the combustor inlet at ground is higher than at cruise altitude. Moreover, engines at ground are operating with higher fuel/air ratios than during cruise. At ground, with $T_0 = 1250$ K, $P_0 = 4.5$ MPa at combustor inlet and $P = 0.082$ MPa and $T \approx 750$ K at engine exit, and $\phi = 0.33$, the model calculates a positive ion concentration at engine exit of about $9.4{\cdot}10^7$ cm^{-3}, about 70 times larger than at cruise. This result is larger than the total negative CI concentration of $1.4{\cdot}10^7$ cm^{-3} measured with a mass spectrometer and a little less than the total positive CI concentration of $1.6{\cdot}10^8$ cm^{-3} measured with an electrostatic probe about 10 ms behind the ATTAS jet engine at ground [2,4]. For $\phi = 0.25$ at ground, the computed total ion number density at combustor exit is about $1.7{\cdot}10^9$ cm^{-3}, i.e. the reduction of ϕ from 0.33 to 0.25 decreases positive ions at engine exit to about $3.8{\cdot}10^7$ cm^{-3}, still 30 times larger than at cruise.

Our calculations (see Table 2) show also that the ion composition depends on the fuel sulfur content. An increase of FSC results in a significant, but less than linear decrease

Table 3
Postcombustor flow age, temperature, pressure, and gas composition mixing ratios at the different sections of a *RB211* engine under cruise conditions of a *B-747* aircraft with $FSC = 0.3\%$

	Combustor exit	High pressure turbine exit	Middle pressure turbine exit	Low pressure turbine exit	Exit nozzle plane
t, ms	0	0.45	1.8	3.2	4.6
T, K	1540	1330	1100	650	598
P, MPa	1.1	0.56	0.25	0.027	0.022
O	8.43(−6)	1.34(−6)	5.94(−7)	1.30(−7)	4.47(−8)
O_2	1.54(−1)	1.54(−1)	1.54(−1)	1.54(−1)	1.54(−1)
O_3	4.30(−9)	2.15(−9)	3.49(−9)	5.37(−8)	9.17(−8)
H	5.25(−8)	1.86(−9)	3.08(−11)	1.32(−13)	3.10(−14)
H_2	5.23(−7)	9.20(−8)	2.59(−8)	2.16(−8)	2.15(−8)
OH	1.40(−4)	3.42(−5)	1.42(−5)	3.08(−6)	1.71(−6)
HO_2	1.01(−6)	3.46(−8)	6.93(−9)	4.22(−8)	3.19(−8)
H_2O	3.99(−2)	3.99(−2)	3.99(−2)	3.99(−2)	3.99(−2)
N	2.56(−13)	1.64(−15)	4.17(−17)	2.01(−20)	4.09(−21)
N_2	7.74(−1)	7.74(−1)	7.74(−1)	7.74(−1)	7.74(−1)
NO	1.13(−4)	1.21(−4)	1.25(−4)	1.23(−4)	1.23(−4)
NO_2	5.39(−5)	4.64(−5)	4.23(−5)	4.30(−5)	4.35(−5)
NO_3	7.89(−11)	2.23(−10)	3.68(−9)	2.49(−8)	2.16(−8)
HNO	6.10(−11)	1.85(−12)	2.79(−13)	6.47(−13)	3.95(−13)
HNO_2	1.96(−8)	5.83(−8)	2.94(−7)	1.40(−6)	1.57(−6)
HNO_3	2.53(−9)	6.80(−9)	2.73(−8)	6.20(−10)	3.90(−10)
N_2O	7.92(−7)	7.82(−7)	7.59(−7)	7.58(−7)	7.58(−7)
NH_3	3.42(−14)	6.97(−15)	1.20(−15)	1.08(−15)	1.08(−15)
CO	2.18(−6)	1.44(−6)	9.46(−7)	9.19(−7)	9.16(−7)
CO_2	3.14(−2)	3.14(−2)	3.14(−2)	3.14(−2)	3.14(−2)
SO	1.75(−10)	1.27(−11)	2.11(−12)	1.27(−14)	1.29(−15)
SO_2	4.25(−5)	4.22(−5)	4.15(−5)	4.00(−5)	3.94(−5)
SO_3	4.88(−7)	7.74(−7)	1.47(−6)	2.87(−6)	3.13(−6)
HSO_3	2.23(−10)	2.14(−10)	4.89(−10)	1.53(−9)	8.79(−10)
H_2SO_4	4.69(−11)	1.82(−10)	1.00(−9)	1.34(−7)	4.63(−7)
H_3O^+	1.61(−14)	1.54(−14)	1.49(−14)	1.49(−14)	1.49(−14)
NO^+	4.65(−13)	4.67(−13)	4.67(−13)	4.67(−13)	4.67(−13)
NO_2^+	1.24(−15)	4.83(−16)	1.69(−16)	5.72(−18)	2.80(−18)
$C_2H_3O^+$	2.91(−13)	2.91(−13)	2.91(−13)	2.91(−13)	2.91(−13)
NO_2^-	1.26(−18)	4.66(−18)	1.21(−17)	1.42(−17)	1.32(−17)
NO_3^-	1.35(−17)	1.29(−17)	1.25(−17)	1.10(−17)	7.13(−19)
SO_2^-	1.60(−18)	1.60(−18)	1.60(−18)	1.60(−18)	1.60(−18)
SO_3^-	1.03(−16)	1.00(−16)	9.20(−17)	8.36(−17)	8.34(−17)
SO_4^-	5.55(−20)	5.31(−20)	4.71(−20)	4.09(−20)	4.08(−20)
HSO_4^-	7.73(−13)	7.73(−13)	7.73(−13)	7.73(−13)	7.73(−13)
CO_3^-	6.44(−20)	5.43(−21)	3.00(−21)	3.64(−22)	9.46(−23)
CO_4^-	9.00(−20)	4.50(−20)	4.73(−20)	2.92(−20)	1.14(−20)

A(n) corresponds $A \cdot 10^n$.

of NO_3^- and NO_2^- concentrations and a slight increase of NO^+ and HSO_4^- concentrations at nozzle exit.

4.2. *The conversion of fuel sulfur to SO_3 and H_2SO_4*

In this section we compare our model with that used in a previous study [58] and investigate the sensitivity of the conversion fraction ε to the initial conversion of SO_2 to SO_3 inside the combustor and to the thermodynamic profiles between combustor exit and engine exit. The previous study investigated the sulfur conversion chemistry in the turbine of a *JT9D-7A* engine, as used on older B747 aircraft, for which measurements had been reported previously for $FSC = 0.0085\%$ [59]. The combustor exit temperature and pressure for this engine are $T_c = 1200$ K and $P_c = 0.77$ MPa. In the box model the temperature and pressure profiles between combustor exit and engine exit have to be prescribed. The previous study assumed a linear temperature profile and a hyperbolic pressure profile as a function of time approaching 621 K and $P_c = 301$ hPa at nozzle exit. In this paper, we use the same initial conditions at combustor exit with gas composition as given in column 2 of Table 4. Using our kinetic scheme in such a box model gives a conversion fraction $\varepsilon = 3.3\%$. This value is close to the result $\varepsilon = 3.8\%$ obtained earlier [58]. In view of small differences in the model kinetics and the high sensitivity of such models to the kinetics, in particular to the reaction rate of SO_2 with OH, this is to be considered a good agreement. If the same model is

Table 4
Gas species mole fractions and conversion fraction ε at combustor exit and at engine exit for a *JT9D-7A* engine computed with the present kinetic model and with prescribed combustor exit data and temperature and pressure profiles inside the turbine duct as used in a previous study [58]

Species	Combustor exit	Engine exit
H	5.06(−18)	6.44(−10)
H_2	2.03(−15)	1.82(−7)
O	1.80(−7)	6.68(−8)
O_2	1.98(−1)	1.98(−1)
OH	9.01(−6)	2.69(−6)
HO_2	4.05(−8)	2.43(−9)
H_2O	3.14(−2)	3.14(−2)
N_2	7.38(−1)	7.38(−1)
NO	2.20(−4)	2.07(−4)
NO_2	4.15(−5)	5.37(−5)
NO_3	2.03(−20)	2.40(−8)
HNO	2.03(−19)	4.78(−14)
HNO_2	2.03(−20)	3.45(−7)
HNO_3	2.03(−20)	1.63(−9)
N_2O	2.03(−20)	5.96(−10)
CO	1.44(−5)	1.42(−5)
CO_2	3.22(−2)	3.22(−2)
CH_4	2.62(−6)	2.01(−6)
SO_2	1.20(−6)	1.16(−6)
SO_3	2.03(−19)	3.87(−8)
HSO_3	2.03(−25)	3.09(−11)
H_2SO_4	2.03(−19)	5.67(−10)
ε, %	0	3.27

A(n) corresponds $A{\cdot}10^n$.

run with initial conditions taken from our combustor model, with 0.69% of the sulfur molecules converted to SO_3 already at combustor exit, the model computes $\varepsilon = 3.92\%$ at nozzle exit, which is 0.65% more than with zero initial SO_3. This confirms that the initial SO_3 adds about linearly to the amount of $SO_3 + H_2SO_4$ available at engine exit.

In order to determine the influence of the temperature profile in the turbine on the sulfur chemistry, we run our kinetic model for the *RB211* engine using either the temperature profile computed by our Q1D model or a linearly decreasing temperature profile. The two cases were run for the combustor exit conditions listed in column 2 of Table 3. For the linear temperature profile, the model computes $\varepsilon = 2.72\%$; for the temperature profile from the Q1D model, the result is $\varepsilon = 8.36\%$. The differences in S-containing gas concentrations and the conversion fraction caused by the linear approximation in comparison to the nonlinear model are significant (up to a factor of 3). A strong impact of flow dynamics and the temperature profile on ε has been found also by others [36,39].

5. Conclusions

The formation of gaseous sulfate aerosol precursors and ions in the combustor and in the turbine of an aircraft engine has been simulated. The combustor model simulates the transient combustion of S-containing hydrocarbon fuels with air in a closed adiabatic reactor under conditions close to those in aircraft engine combustors. The turbine flow is computed with a quasi one-dimensional flow model. Both models include new gas species and ion kinetic models. This is the first published model study of ion formation inside an aircraft engine.

The concentrations of ions depend strongly on the fuel/air equivalence ratio ϕ and also, but less than linearly, on the fuel sulfur content. The total ion mole fraction stays close to constant in the turbine section of the engine in this model. The computed positive ion (mainly NO^+) concentrations at engine exit of $1.39{\cdot}10^6$ cm^{-3} for cruise regime is 100 times less than the concentration expected from positive ion measurements at the ground with an electrostatic probe [4]. The corresponding total ion concentration of about $4.5{\cdot}10^6$ cm^{-3} corresponds to a total ion emission index of $2{\cdot}10^{15}$ kg^{-1}. This value is also 100 times less than what has been derived from aerosol measurements with CI-driven nucleation models [29]. For ground conditions, with higher pressure and temperature at combustor inlet and higher fuel/air ratio, the computed total number density of positive and negative ions is 70 times larger and about $\sim 10^8$ cm^{-3} which is not far off the value measured [4]. This indicates a strong dependence of CI emission on the type and operation of the engines.

Larger ion concentrations would occur, in particular in the combustor, if the recombination rate in the combustor is smaller than assumed in the model. Also peculiarities of turbulent combustion with locally inhomogeneous fuel/air ratios in the various parts of the combustor are expected to cause larger ion concentrations. This needs to be investigated with three-dimensional combustion models in the future. Finally, further important CI formation processes may exist which are not included in the model. Because of self-limitation of the ion concentration by recombination, the engine dependence could be weaker for higher CI emissions from the combustor.

Most of the relevant H-, N- and some of the S-species do not reach chemical equilibrium in the combustors. Most of the oxidation of fuel sulfur to SO_3 and H_2SO_4 occurs in the turbine between the combustor and engine exit. A small fraction of the SO_3 is formed already inside the combustor. The conversion in the combustor adds about linearly to the ε value at engine exit. The sulfur conversion fraction ε in an *RB211* engine is computed by this model to be $\approx 9\%$, and $\approx 8.4\%$, for FSC of 0.04% and 0.3%, respectively. Hence, an increase in FSC causes a minor reduction in ε. The results of the present sulfur chemistry kinetics agree well with those of a previous study [58] if applied with the same temperature and pressure profiles and the same initial conditions, though both models may suffer from uncertainties in the sulfur kinetics. The sulfur conversion fraction ε depends strongly on the temperature profile along the flow within the engine. The assumption of a linear temperature profile in the turbine may cause an underestimate of ε by a factor of 3.

Acknowledgements

This work was supported within the CHEMICON project by the Environment and Climate Research Program of EC under grant ENV4-CT97-0620 and by the Russian Foundation for Basic Research under grant 99-01-01165. We thank Hans Georg Tremmel for providing details of his calculation results for comparison and Frank Arnold and Reinhold Zellner for helpful discussions.

Appendix A. Kinetic mechanisms

Table A1
Kinetic mechanism for S-containing gas species formation

No.	Reaction		K_{+f} $(\mathrm{cm}^3/\mathrm{mol})^{m-1}\ \mathrm{s}^{-1}$		
			A_f	n_f	E_{af}
			Reactions with S, S_2, S_4		
1.	$S + S + M = S_2 + M$		3.98(17)	−1	−171
2.	$S_2 + S_2 + M = S_4 + M$		9.09(16)	0	0
			Reactions with HS, H_2S		
3.	$HS + HS = H_2 + S_2$		1.29(14)	0	0
4.	$HS + HS = H_2S + S$		7.04(12)	0	0
5.	$H + HS = H_2 + S$		1.51(13)	0	0
6.	$S + HS = H + S_2$		2.69(13)	0	0
7.	$S + H_2S = H_2 + S_2$		6.14(12)	0	−2514
8.	$H_2S + M = H + HS + M$		7.94(25)	−2	−46 255
9.	$H_2S + H = H_2 + HS$		7.77(12)	0	−865
10.	$H_2S + O = HS + OH$		4.36(12)	0	−1679
11.	$H_2S + OH = H_2O + HS$		1.38(13)	0	−447
			Reactions with SO, SO_2, S_2O		
12.	$S + O_2 = SO + O$		6.32(11)	0.5	0
13.	$S_2 + O = S + SO$		6.32(11)	0.5	0
14.	$HS + O_2 = SO + OH$		1.23(11)	0	−1750
15.	$HS + O = H + SO$		3.55(14)	0	−327
16.	$SO + O + M = SO_2 + M$	k_+	6.91(16)	0	0
		k_-	2.90(16)	0	−59 200
17.	$SO + O_2 = SO_2 + O$		4.46(11)	0	−3268
18.	$SO + OH = SO_2 + H$		1.82(13)	0	0
19.	$SO + SO = SO_2 + S$		3.50(12)	0	−1760
20.	$S_2 + SO = S_2O + S$		4.00(13)	0	−12 594
21.	$S_2O + O = S_2 + O_2$		1.00(10)	0	0
22.	$S + SO_2 = S_2O + O$		3.98(13)	0	−22 795
23.	$S + OH = SO + H$		4.00(13)	0	0
24.	$S + O + M = SO + M$		4.60(17)	−1	−87
25.	$S + NO_2 = SO + NO$		2.95(13)	0	84
26.	$SO + NO_2 = SO_2 + NO$		8.91(12)	0	0
27.	$S + O_3 = SO + O_2$		7.30(12)	0	0
28.	$SO + O_3 = SO_2 + O_2$		1.50(12)	0	−1056
			Reactions with SO_3		
29.	$SO_2 + O + M = SO_3 + M$	k_+	4.40(14)	0	−3196
		k_-	3.16(15)	0	−32 201
30.	$SO + SO_3 = SO_2 + SO_2$		1.20(9)	0	0
31.	$SO_3 + O = SO_2 + O_2$		6.50(14)	0	−5456
32.	$SO_2 + NO_2 = SO_3 + NO$		6.31(12)	0	−13 729
33.	$CH_3O_2 + SO_2 = CH_3O + SO_3$		3.01(7)	0	0
			Reactions with HSO, HSO_2, HSO_3, H_2SO_4		
34.	$HS + NO_2 = HSO + NO$		1.75(13)	0	−240
35.	$HS + O_3 = HSO + O_2$		5.72(12)	0	−280
36.	$HSO + NO_2 = HSO_2 + NO$		5.78(12)	0	0
37.	$HSO_2 + O_2 = HO_2 + SO_2$		1.81(11)	0	0
38.	$SO_2 + OH = HSO_3$		9.03(11)	0	0
39.	$HSO_3 + O_2 = HO_2 + SO_3$		7.83(11)	0	−333

Table A1 (*—continued*)

No.	Reaction	K_{+f} (cm^3/mol)$^{m-1}$s^{-1}		
		A_f	n_f	E_{af}
40.	$SO_3 + H_2O = H_2SO_4$	7.23(8)	0	0
41.	$HSO + O_3 = HS + O_2 + O_2$	6.03(10)	0	0
	Reactions with CS, CS_2, COS			
42.	$CO + S + M = COS + M$	2.05(16)	0	−910
43.	$CO + SO = CO_2 + S$	3.98(13)	0	−12 569
44.	$CO + SO_2 = CO_2 + SO$	3.98(11)	0	−12 569
45.	$COS + O = CO + SO$	1.90(13)	0	−2278
46.	$COS + S = CO + S_2$	1.70(12)	0	−2061
47.	$COS + H = CO + HS$	1.29(10)	0	0
48.	$CS + O_2 = CO + SO$	5.49(10)	0	−1016
49.	$CS + O_2 = COS + O$	1.00(13)	0	−6078
50.	$CS + SO = CO + S_2$	1.00(9)	0	0
51.	$CS_2 + O = CS + SO$	5.01(13)	0	−960
52.	$CS_2 + O = COS + S$	1.00(14)	0	−4052
53.	$CS_2 + O = S_2 + CO$	1.20(12)	0	−523
54.	$CS_2 + S = CS + S_2$	1.00(14)	0	−2026
55.	$CS_2 + O_2 = CS + SO_2$	1.00(12)	0	−2212
56.	$C + S + M = CS + M$	2.00(18)	−1	0
57.	$CS + S + M = CS_2 + M$	2.00(16)	0	−905
58.	$O + CS = CO + S$	1.63(14)	0	−760
59.	$CS + O_3 = COS + O_2$	1.81(8)	0	0
60.	$CS + NO_2 = COS + NO$	4.58(7)	0	0
61.	$OH + CS_2 = HS + COS$	1.20(9)	0	0

A(n) corresponds to A·10^n. $K_f = A_f \cdot T^{n_f} \exp(E_{af}/T)$, m is the number of molecules participating in the reaction. Reactions (1)–(22), (34)–(37), (42)–(55), (58)–(61) were taken from [44]; (23), (29)–(31), (40) from [9]; (24)–(26), (41) from [26]; (27)–(28), (56)–(57) from [47]; (32) from [60]; (33) from [36]; (38), (39) from [16].

Table A2
Reaction mechanism for chemi-ions formation during combustion of S-containing hydrocarbons and air mixtures

No.	Reaction	k^+			k^-			Ref.
		A	n	E_a	A	n	E_a	
	Reactions with CH($a^4\Sigma^-$)							
1.	$C_2H + O_2 = CH(a^4\Sigma^-) + CO_2$	4.5(15)	0	12 635	2.75(16)	0	20 934	[17]
2.	$C_2H + O = CH(a^4\Sigma^-) + CO$	7.1(11)	0	0	3.55(11)	0	4756	[17]
3.	$C_2 + OH = CH(a^4\Sigma^-) + CO$	3.39(12)	0	0	1.2(13)	0	22 885	[17]
4.	$CH(a^4\Sigma^-) + M = CH + M$	4(10)	0.5	0	4(10)	0.5	25 018	[17]
5.	$CH(a^4\Sigma^-) + O_2 = CH + O_2$	2.4(12)	0.5	0				[41]
6.	$CH(a^4\Sigma^-) = CH$	1.95(6)	0	0	1.95(6)	0	25 018	[17]
7.	$CH(a^4\Sigma^-) + H = C + H_2$	1.51(14)	0	0	5.25(14)	0	36 678	[17]
8.	$CH(a^4\Sigma^-) + O = CO + H$	5.75(13)	0	0	3.98(−15)	3	35 136	[17]
9.	$CH(a^4\Sigma^-) + OH = C + H_2O$	3.02(13)	0	0	4.9(14)	0	44 340	[17]
10.	$CH(a^4\Sigma^-) + CH_3 = C_2H_3 + H$	3.02(13)	0	0	7.41(3)	3	48 697	[17]
11.	$CH(a^4\Sigma^-) + O_2 = CO + OH$	1.35(14)	0.67	12 989	2.75(−11)	3	50 344	[17]
12.	$CH(a^4\Sigma^-) + O_2 = HCO + O$	1(16)	0	0	1.66(3)	3	49 884	[17]
	Associative ionization							
13.	$CH + O = HCO^+ + e$	2.5(11)	0	854.4	5.75(24)	−2.3	3240	[17]
14.	$CH(a^4\Sigma^-) + O = HCO^+ + e$	5.01(14)	0	859	9.55(19)	0	25 771	[17]
15.	$CH(a^4\Sigma^-) + C_2H_2 = C_3H_3^+ + e$	2(11)	0	0	3.47(25)	−2.7	−3351	[17]
16.	$C_2 + CH_3 = C_3H_3^+ + e$	1(10)	0	0	4.37(25)	−3	−8723	[17]
17.	$N + N = N_2^+ + e$	1.57(8)	1.38	66 300	1.82(20)	−0.93	196	[37]
18.	$N + O = NO^+ + e$	1.56(7)	1.43	31 143	1.38(18)	−0.45	59	[37]
19.	$O + O = O_2^+ + e$	2.42(9)	0.87	79 214	3.89(22)	−1.62	40	[37]
	Dissociative ionization							
20.	$O_3 + e = O_2^- + O$	6(14)	0	0	9(13)	0	0	[35]

Table A2 (*—continued*)

No.	Reaction	k^+			k^-			Ref.
		A	n	E_a	A	n	E_a	
21.	$N_2O + e = N_2 + O^-$	1.2(14)	0	0	1.2(5)	0	0	[55]
22.	$HNO_3 + e = NO_2^- + OH$	3(16)	0	0				[30]
23.	$CO + e = C + O^-$	1.8(10)	0	0	0	0	0	[55]
	Ionization under molecule and electron interaction							
24.	$N_2 + e = N_2^+ + e + e$	2.19(−8)	5.04	180 840	1.5(5)	2.56	2446	[37]
25.	$N + e = N^+ + e + e$	1.8(13)	0.6	168 772	2.61(19)	−0.5	−6663	[37]
26.	$NO + e = NO^+ + e + e$	6.46(23)	−1.68	107 367	1.96(33)	−3.34	418	[37]
27.	$O_2 + e = O_2^+ + e + e$	1(-13)	6.02	140 150	9.40(−3)	3.84	3478	[37]
28.	$O + e = O^+ + e + e$	5.2(12)	0.68	157 981	1(22)	−1.04	−4544	[37]
	Associative electron attachment							
29.	$NO_2 + e = NO_2^-$	1.8(13)	0	0				[35]
30.	$NO + e + M = NO^- + M$	3.6(17)	0	0	0	0	0	[35]
31.	$O_2 + e + O = O_2^- + O$	3.6(16)	0	0				[35]
32.	$O_2 + e + O_2 = O_2^- + O_2$	1.51(21)	−1	600	9.35(12)	0.5	5590	[35]
33.	$O_2 + e + N_2 = O_2^- + N_2$	3.47(21)	−2	70	6.58(10)	0.5	4990	[35]
34.	$O + e + N_2 = O^- + N_2$	3.6(16)	0	0				[55]
35.	$O + e + O_2 = O^- + O_2$	3.6(16)	0	0				[35]
	Nonresonance charge exchange							
	a) Positive ions							
36.	$N_2^+ + NO_2 = NO_2^+ + N_2$	1.8(14)	0	0				[42]
37.	$N^+ + N_2 = N_2^+ + N$	1(12)	0.5	12 199	1.37(17)	−0.83	3048	[37]
38.	$N^+ + NO = N + NO^+$	5.4(14)	0	0				[42]
39.	$N^+ + O = O^+ + N$	3.39(5)	1.58	0	4.65(8)	0.96	12 185	[37]
40.	$NO^+ + N_2 = NO + N_2^+$	3.8(15)	0	73 231	1.47(17)	−0.72	765	[37]
41.	$NO^+ + O_2 = NO + O_2^+$	2.4(13)	0.41	32 600	6.44(13)	0.13	456	[37]
42.	$NO^+ + O = NO + O^+$	1.82(13)	0	50 129	1.21(13)	−0.06	−460	[37]
43.	$NO_2^+ + NO = NO^+ + NO_2$	1.74(14)	0	0				[35,42]
44.	$O_2^+ + N_2 = O_2 + N_2^+$	9.91(12)	0	40 700	1.44(14)	−0.44	379	[37]
45.	$O_2^+ + N = O_2 + N^+$	8.71(13)	0.14	28 599	1.57(10)	0.98	−2030	[37]
46.	$O_2^+ + NO_2 = NO_2^+ + O_2$	5.28(14)	0	0				[42]
47.	$O_2^+ + O = O_2 + O^+$	4(12)	−0.09	18 000	9.84(11)	0.13	−424	[37]
48.	$O^+ + N_2 = O + N_2^+$	9(11)	0.36	22 799	5.18(13)	−0.3	926	[37]
49.	$O^+ + NO_2 = NO_2^+ + O$	9.6(14)	0	0				[35,42]
50.	$O_4^+ + NO = NO^+ + O_2 + O_2$	6(13)	0	0	0	0	0	[35]
51.	$H_2O^+ + O_2 = O_2^+ + H_2O$	1.2(14)	0	0				[21]
52.	$N_2^+ + NH_3 = NH_3^+ + N_2$	1.14(15)	0	0	0	0	0	[42]
53.	$N^+ + NH_3 = NH_3^+ + N$	1.44(15)	0	0	0	0	0	[42]
54.	$O_2^+ + NH_3 = NH_3^+ + O_2$	6(14)	0	0	0	0	0	[42]
55.	$N_2^+ + CO = CO^+ + N_2$	4.2(13)	0	0				[21]
56.	$N_2^+ + CO_2 = CO_2^+ + N_2$	5.4(14)	0	0				[21]
57.	$N^+ + CO = CO^+ + N$	3(14)	0	0				[21]
58.	$N^+ + CO_2 = CO_2^+ + N$	7.8(14)	0	0				[21]
59.	$CO^+ + O_2 = O_2^+ + CO$	1.2(14)	0	0				[21]
60.	$CO^+ + CO_2 = CO_2^+ + CO$	6.6(14)	0	0				[21]
61.	$CO_2^+ + NO = NO^+ + CO_2$	7.2(13)	0	0				[42]
62.	$CO_2^+ + O_2 = O_2^+ + CO_2$	3.36(13)	0	0				[42]
	b) Negative ions							
63.	$NO^- + NO_2 = NO_2^- + NO$	4.44(14)	0	0	0	0	0	[30]
64.	$NO^- + O_2 = O_2^- + NO$	5.4(14)	0	0	0	0	0	[21]
65.	$NO_2^- + NO_3 = NO_2 + NO_3^-$	3(14)	0	0				[35]
66.	$O_2^- + NO_2 = NO_2^- + O_2$	4.2(14)	0	0				[30,42]
67.	$O_2^- + NO_3 = NO_3^- + O_2$	3(14)	0	0				[35]

Table A2 (*—continued*)

No.	Reaction	k^+			k^-			Ref.
		A	n	E_a	A	n	E_a	
68.	$O_2^- + O = O^- + O_2$	1.98(14)	0	0				[35]
69.	$O_2^- + O_3 = O_3^- + O_2$	1.8(14)	0	0	0	0	0	[21]
70.	$O^- + NO_2 = NO_2^- + O$	7.2(14)	0	0	0	0	0	[21,35]
71.	$O^- + O_3 = O_3^- + O$	4.2(14)	0	0	0	0	0	[21]
72.	$O^- + N_2O = N_2O^- + O$	1.2(12)	0	0	0	0	0	[35]
73.	$O_3^- + NO_2 = NO_2^- + O_3$	4.2(14)	0	0	0	0	0	[21,35]
74.	$O_3^- + NO_3 = O_3 + NO_3^-$	3(14)	0	0	0	0	0	[35]
75.	$H^- + NO_2 = NO_2^- + H$	3(14)	0	0				[21]
76.	$OH^- + NO_2 = NO_2^- + OH$	6(14)	0	0				[21]
77.	$OH^- + O_3 = O_3^- + OH$	5.4(14)	0	0	0	0	0	[30]
78.	$O_2^- + SO_2 = SO_2^- + O_2$	3.24(14)	0	0	0	0	0	[21]
	Binary ion–molecular reactions							
	a) Positive ions							
79.	$N_2^+ + NO_2 = NO^+ + N_2O$	3(13)	0	0				[42]
80.	$N_2^+ + O = NO + N^+$	1.82(14)	0	25761	6.71(9)	1	−1994	[37]
81.	$N^+ + NO = O^+ + N_2$	6(11)	0	0				[35]
82.	$N^+ + O_2 = O^+ + NO$	2.16(13)	0	0				[42]
83.	$N^+ + O_3 = NO^+ + O_2$	3(14)	0	0				[35]
84.	$N^+ + N_2O = NO^+ + N_2$	3.3(14)	0	0				[35]
85.	$NO^+ + N = N_2 + O^+$	3.39(13)	−1.08	12 800	6.81(12)	−0.85	−346	[37]
86.	$NO^+ + N = N_2^+ + O$	7.24(13)	0	35 500	9.51(14)	−0.43	478	[37]
87.	$NO^+ + NO = N_2 + O_2^+$	3.24(8)	0	11 947	3.6(10)	−0.37	1885	[37]
88.	$NO^+ + NO = O_2 + N_2^+$	1.1(11)	0	51 529	1.76(14)	−0.81	1148	[37]
89.	$NO^+ + O = N^+ + O_2$	1(12)	0.5	77 201	5.9(10)	0.68	−935	[37]
90.	$NO^+ + O = O_2^+ + N$	7.76(12)	0.29	48 599	2.54(15)	−0.37	1095	[37]
91.	$NO^+ + O_3 = NO_2^+ + O_2$	6(8)	0	0				[35]
92.	$O_2^+ + NO_2 = NO^+ + O_3$	6(12)	0	0				[35]
93.	$O^+ + NO = O_2^+ + N$	1.8(12)	0	0				[35]
94.	$O^+ + O_3 = O_2^+ + O_2$	3(14)	0	0				[35]
95.	$O^+ + N_2O = NO^+ + NO$	1.38(14)	0	0				[35]
96.	$O^+ + N_2O = O_2^+ + N_2$	1.2(13)	0	0				[35]
97.	$HCO^+ + H_2O = H_3O^+ + CO$	1(16)	−0.0897	0	3.09(16)	−0.0897	15021	[17]
98.	$H_2O^+ + H_2O = H_3O^+ + OH$	5.1(14)	0	0				[21]
99.	$H_3O^+ + CH_2O = CH_2OH^+ + H_2O$	1.32(15)	0	0	4.38(14)	0	2626	[20]
100.	$NH_3^+ + NH_3 = NH_4^+ + NH_2$	1.32(15)	0	0	0	0	0	[42]
101.	$H_3O^+ + NH_3 = NH_4^+ + H_2O$	1.5(15)	0	0				[42]
102.	$CH_4 + N_2^+ = CH_3^+ + N_2H$	7.2(14)	0	0				[5]
103.	$CH_4 + N^+ = CH_3^+ + NH$	3.3(14)	0	0				[5]
104.	$CH_4 + O^+ = CH_3^+ + OH$	3(14)	0	0				[5]
105.	$O^+ + CO_2 = O_2^+ + CO$	7.2(14)	0	0				[21]
106.	$C^+ + O_2 = CO^+ + O$	6(14)	0	0				[21]
107.	$C^+ + CO_2 = CO^+ + CO$	1.14(15)	0	0				[21]
108.	$H_3O^+ + CH_2 = CH_3^+ + H_2O$	6.17(14)	−0.006	0	7.41(14)	−0.006	14591	[17]
109.	$H_3O^+ + C_2H_2 = C_2H_3O^+ + H_2$	8.39(15)	0	0				[41]
110.	$HCO^+ + CH_2 = CH_3^+ + CO$	5.62(14)	−0.006	0	2.09(15)	−0.006	29612	[17]
111.	$HCO^+ + C_2H_2 = C_2H_3^+ + CO$	7.08(14)	0	0	1.95(14)	0	8122	[17]
112.	$HCO^+ + C_2H_3 = C_3H_3^+ + OH$	7.59(14)	−0.074	0	3.39(3)	3	−1931	[17]
113.	$CH_3^+ + CO_2 = C_2H_3O^+ + O$	7.24(14)	0	0				[41]
114.	$CH_3^+ + C_2H_2 = C_3H_3^+ + H_2$	7.24(14)	0	0	1.66(15)	0	29471	[17]
115.	$C_2H_3^+ + H_2O = H_3O^+ + C_2H_2$	6.92(15)	0	0	7.76(16)	0	6894	[17]
116.	$C_3H_3^+ + H_2O = C_2H_3O^+ + CH_2$	7.24(14)	0	0				[41]
117.	$C^+ + N_2O = NO^+ + CN$	5.46(14)	0	0				[55]
118.	$N^+ + CO_2 = NO^+ + CO$	1.08(13)	0	0				[55]
119.	$CO^+ + H_2 = HCO^+ + H$	1.2(15)	0	0				[55]
120.	$N_2^+ + O_3 = O_2^+ + O + N_2$	6(13)	0	0				[35]
121.	$N_2^+ + N_2O = NO^+ + N_2 + N$	2.4(14)	0	0				[35]

Table A2 (*—continued*)

No.	Reaction	k^+			k^-			Ref.
		A	n	E_a	A	n	E_a	
122.	$O_4^+ + O = O_2^+ + O_3$	1.8(14)	0	0	0	0	0	[35]
	b) Negative ions							
123.	$NO^- + N_2O = NO_2^- + N_2$	1.68(10)	0	0	0	0	0	[35]
124.	$NO_2^- + NO_2 = NO_3^- + NO$	6(10)	0	0	3(11)	0	0	[42]
125.	$NO_2^- + N_2O = NO_3^- + N_2$	3(11)	0	0				[42]
126.	$NO_2^- + HNO_3 = NO_3^- + HNO_2$	9.6(14)	0	0				[19,30,42]
127.	$NO_2^- + O_3 = NO_3^- + O_2$	7.2(13)	0	0				[42]
128.	$N_2O^- + O_2 = O_3^- + N_2$	6(14)	0	0	0	0	0	[21]
129.	$O_2^- + NO = NO_2^- + O$	6(11)	0	0				[55]
130.	$O_2^- + N_2O = NO_2^- + NO$	1.2(10)	0	0				[30]
131.	$O_2^- + N_2O = O_3^- + N_2$	6(12)	0	0	0	0	0	[55]
132.	$O^- + NO_2 = O_2^- + NO$	1.08(13)	0	0				[21]
133.	$O^- + N_2O = O_2^- + N_2$	1.32(14)	0	0				[30]
134.	$O^- + N_2O = NO^- + NO$	1.2(14)	0	0	0	0	0	[8,55]
135.	$O_3^- + N_2 = NO_2^- + NO$	3(10)	0	0	0	0	0	[55]
136.	$O_3^- + NO = NO_2^- + O_2$	1.56(12)	0	0	0	0	0	[35]
137.	$O_3^- + NO = NO_3^- + O$	6(12)	0	0	0	0	0	[21,35]
138.	$O_3^- + NO_2 = NO_3^- + O_2$	1.68(14)	0	0	0	0	0	[30]
139.	$O_3^- + O = O_2^- + O_2$	1.92(14)	0	0	0	0	0	[35]
140.	$O^- + H_2 = OH^- + H$	3.6(13)	0	0				[30]
141.	$O^- + H_2O = OH^- + OH$	3.6(11)	0	0				[30]
142.	$O^- + CH_4 = CH_3 + OH^-$	9.15(14)	−0.5	0				[19,54]
143.	$O^- + C_2H_6 = C_2H_5 + OH^-$	6.13(15)	−0.5	0				[19,54]
144.	$O^- + HCN = CN^- + OH$	2.22(15)	0	0				[30]
145.	$OH^- + HCN = CN^- + H_2O$	2.46(15)	0	0				[30]
146.	$O_3^- + CO_2 = CO_3^- + O_2$	3.3(14)	0	0	3.6(9)	0	0	[30]
147.	$O_4^- + NO = NO_3^- + O_2$	1.5(14)	0	0	0	0	0	[30]
148.	$O_4^- + O = O_3^- + O_2$	2.4(14)	0	0	0	0	0	[35]
149.	$O_4^- + CO = CO_3^- + O_2$	1.2(13)	0	0	0	0	0	[30]
150.	$O_4^- + CO_2 = CO_4^- + O_2$	2.58(14)	0	0	0	0	0	[30]
151.	$CO_3^- + NO = NO_2^- + CO_2$	5.4(12)	0	0	0	0	0	[21]
152.	$CO_3^- + NO_2 = NO_3^- + CO_2$	4.8(13)	0	0	0	0	0	[21]
153.	$CO_3^- + O = O_2^- + CO_2$	4.8(13)	0	0	0	0	0	[21]
154.	$CO_3^- + N_2O = CO_4^- + N_2$	3(11)	0	0	0	0	0	[30]
155.	$CO_4^- + NO = NO_3^- + CO_2$	2.88(13)	0	0	0	0	0	[30]
156.	$CO_4^- + O = CO_3^- + O_2$	9(13)	0	0	0	0	0	[55]
157.	$CO_4^- + O = O_3^- + CO_2$	6(13)	0	0	0	0	0	[55]
158.	$CO_4^- + O_3 = O_3^- + CO_2 + O_2$	7.8(13)	0	0	0	0	0	[30]
159.	$NO_3^- + O_3 = NO_2^- + O_2 + O_2$	6(10)	0	0				[30]
160.	$O_3^- + SO_2 = SO_3^- + O_2$	1.53(14)	0	0	0	0	0	[21]
161.	$O_3^- + SO_2 = SO_4^- + O$	1.53(14)	0	0	0	0	0	[21]
162.	$SO_4^- + HNO_3 = HSO_4^- + NO_3$	3.6(14)	0	0	0	0	0	[19]
163.	$SO_3^- + HNO_3 = HSO_3 + NO_3^-$	2.4(14)	0	0	0	0	0	[19]
164.	$O^- + H_2SO_4 = HSO_4^- + OH$	2.52(15)	0	0	0	0	0	[30]
165.	$NO_3^- + H_2SO_4 = HSO_4^- + HNO_3$	1.56(15)	0	0	0	0	0	[30]
166.	$CO_3^- + SO_2 = SO_3^- + CO_2$	3.1(17)	−1.27	0	0	0	0	[54]
	Ion–molecular reactions with electron formation							
167.	$NO_2^- + O = NO_3 + e$	6(11)	0	0				[35]
168.	$O_2^- + N = NO_2 + e$	3(14)	0	0				[35]
169.	$O^- + N = NO + e$	1.56(14)	0	0				[35]
170.	$O^- + NO = NO_2 + e$	1.56(14)	0	0				[35]
171.	$O^- + O_2 = O_3 + e$	3(9)	0	0				[35]
172.	$O^- + O = O_2 + e$	3(14)	0	0				[35]
173.	$O^- + H_2 = H_2O + e$	3.48(14)	0	0				[30]
174.	$H^- + O_2 = HO_2 + e$	9(14)	0	0				[55]
175.	$H^- + H = H_2 + e$	7.8(14)	0	0				[55]
176.	$OH^- + N = HNO + e$	6(12)	0	0				[55]

Table A2 (*—continued*)

No.	Reaction	k^+			k^-			Ref.
		A	n	E_a	A	n	E_a	
177.	$OH^- + O = HO_2 + e$	1.2(14)	0	0				[55]
178.	$OH^- + H = H_2O + e$	6(14)	0	0				[55]
179.	$CN^- + H = HCN + e$	4.8(14)	0	0				[55]
180.	$O^- + CO = CO_2 + e$	3.3(14)	0	0				[30]
181.	$O_2^- + N = NO + O + e$	2.4(14)	0	0				[55]
182.	$O_3^- + O = O_2 + O_2 + e$	1.8(14)	0	0	0	0	0	[35]
183.	$NO^- + CO = e + CO + NO$	3(11)	0	0	0	0	0	[30]
184.	$NO^- + CO_2 = e + CO_2 + NO$	4.98(12)	0	0	0	0	0	[30]
185.	$NO^- + NO = e + NO + NO$	3(12)	0	0	0	0	0	[30]
186.	$NO^- + N_2O = e + NO + N_2O$	3.06(12)	0	0	0	0	0	[30]
187.	$O_3^- + N_2O = e + N_2 + O_2 + O_2$	1.2(10)	0	0	0	0	0	[30]
	Ternary recombination of ion and neutral							
188.	$N^+ + N + M = N_2^+ + M$	2.6(20)	−0.75	0				[12,35]
189.	$N^+ + O + M = NO^+ + M$	2.6(20)	−0.75	0				[12,35]
190.	$O^+ + N + M = NO^+ + M$	2.6(20)	−0.75	0				[12,35]
191.	$O^+ + O + M = O_2^+ + M$	2.6(20)	−0.75	0				[12,35]
192.	$O_2^+ + O_2 + O_2 = O_4^+ + O_2$	7.3(25)	−3.2	0	1.6(28)	−4	5030	[35]
193.	$O_2^- + N + M = NO_2^- + M$	3.6(18)	0	0				[55]
194.	$O^- + NO + M = NO_2^- + M$	3.6(18)	0	0				[35]
195.	$O^- + O_2 + O_2 = O_3^- + O_2$	3.24(17)	0	0	0	0	0	[42]
196.	$O^- + CO_2 + M = CO_3^- + M$	1.12(20)	0	0	0	0	0	[30]
197.	$O_2^- + O_2 + M = O_4^- + M$	3.78(19)	−1	0	6(13)	0	1044	[35]
198.	$O_2^- + CO_2 + M = CO_4^- + M$	1.69(19)	0	0	0	0	0	[30]
199.	$O_4^- + O = O^- + O_2 + O_2$	1.8(14)	0	0	0	0	0	[35]
200.	$CO_3^- + CO = CO_2 + CO_2 + e$	3(11)	0	0	0	0	0	[55]
201.	$O_2^- + O_2 + N_2 = NO_2^- + NO_2$	2.1(6)	0	0				[55]
	Dissociative recombination							
202.	$NO_2^+ + e = NO + O$	2.08(18)	−0.5	0				[35]
203.	$H_3O^+ + e = H_2O + H$	2.29(18)	−0.5	0	7.41(−7)	3	40 453	[17]
204.	$CO_2^+ + e = CO + O$	3.6(16)	0	0				[55]
205.	$CH_3^+ + e = CH_2 + H$	2.29(18)	−0.5	0	3.39(−2)	3	43 779	[17]
206.	$C_2H_3^+ + e = C_2H_2 + H$	2.29(18)	−0.5	0	1.02(−7)	3	39 872	[17]
207.	$C_2H_3O^+ + e = CH_2CO + H$	2.29(18)	−0.5	0	0	0	0	[41]
208.	$C_3H_3^+ + e = C_2H_2 + CH$	1.5(19)	−0.5	0	0	0	0	[41]
209.	$O_4^+ + e = O_2 + O_2$	1.46(19)	−0.5	0	0	0	0	[35]
	Ion-electron recombination							
210.	$NO_2^+ + e = NO_2$	1.2(19)	0	0				[42]
211.	$O^+ + e + O_2 = O + O_2$	1(30)	−3.5	0				[12,35]
212.	$O^+ + e + N_2 = O + N_2$	1(30)	−3.5	0				[12,35]
213.	$HCO^+ + e + e = HCO + e$	3.98(39)	−4.5	0	9.55(−5)	3	37 360	[17]
214.	$CH_3^+ + e + e = CH_3 + e$	3.98(39)	−4.5	0	9.77(−10)	3	30 537	[17]
215.	$C_2H_3^+ + e + e = C_2H_3 + e$	3.98(39)	−4.5	0	6.03(−5)	3	37 304	[17]
	Binary ion–ion recombination							
216.	$A^- + B^+ = A + B$ $A = O_2, O, O_3, NO, NO_2, NO_3, N_2O, SO_2, SO_3, CN$; $B = N_2, O_2, N, O, NO, NO_2, CO, CO_2, NH_3, C_2H_3O$.	2.09(18)	−0.5	0				[35]
217.	$A^- + (BC)^+ = A + B + C$ $A = O_2, O, O_3, NO, NO_2, NO_3, N_2O, SO_2, SO_3, CN$; $(BC) = N_2, O_2, NO, NO_2, O_4, C_2H_3O$.	6.02(16)	0	0				[35]
218.	$(AB)^- + C^+ = A + B + C$ $(AB) = O_4$; $C = N_2, O_2, N, O, NO, NO_2$.	6.02(16)	0	0				[35]
219.	$NO_3^- + NH_4^+ = NO_3 + NH_3 + H$	1.8(18)	0	0				[42]
220.	$O_4^- + O_4^+ = O_2 + O_2 + O_2 + O_2$	6.02(16)	0	0	0	0	0	[35]

Table A2 (*—continued*)

No.	Reaction	k^+			k^-			Ref.
		A	n	E_a	A	n	E_a	
	Ternary ion–ion recombination							
221.	$A^- + B^+ + M = A + B + M$ $M = N_2, O_2$ $A = O_2, O.$ $B = N_2, O_2, N, O, NO$	1.12(29)	−2.5	0				[35]
222.	$A^- + B^+ + M = AB + M$ $M = N_2, O_2$ a) $A = O_2$; $B = N, O, NO$ b) $A = O$; $B = N_2, O_2, N, O, NO$	1.12(29)	−2.5	0				[35]

$k^{+(-)} = a \cdot T^n \exp(-E_a/T)$ cm^3/mol^{m-1} s^{-1}, m is the number of molecules participating in the reaction. B(p) corresponds to B·10^p.

References

[1] F. Arnold, J. Scheid, T. Stilp, H. Schlager, M.E. Reinhardt, Measurements of jet aircraft emissions at cruise altitude, 1, The odd-nitrogen gases NO, NO_2, HNO_2, and HNO_3, Geophys. Res. Lett. 19 (1992) 2421–2424.

[2] F. Arnold, T. Stilp, R. Busen, U. Schumann, Jet engine exhaust chemiion measurements: Implications for gaseous SO_3 and H_2SO_4, Atmos. Env. 32 (1998) 3073–3077.

[3] F. Arnold, K.H. Wohlfrom, M.W. Klemm, J. Schneider, K. Gollinger, U. Schumann, R. Busen, First gaseous ion composition measurements in the exhaust plume of jet aircraft in flight: Implications for gaseous sulfuric acid, aerosols, and chemiions, Geophys. Res. Lett. 25 (1998) 2137–2140.

[4] F. Arnold, A. Kiendler, V. Wiedemer, S. Aberle, T. Stilp, R. Busen, Chemiion concentration measurements in jet engine exhaust at the ground: Implications for ion chemistry and aerosol formation in the wake of a jet aircraft, Geophys. Res. Lett. 27 (2000) 1723–1726.

[5] S.T. Arnold, R.A. Morris, A.A. Viggiano, Reactions of O- with various alkanes: competition between hydrogen abstraction and reactive detachment, J. Phys. Chem. A 102 (1997) 1345–1348.

[6] S. Böckle, S. Einecke, F. Hildenbrand, C. Orlemann, A. Schulz, J. Wolfrum, V. Sick, Laser-spectroscopic investigation of OH-radical concentrations in the exhaust plane of jet engines, Geophys. Res. Lett. 26 (1999) 1849–1852.

[7] G.P. Brasseur, R.A. Cox, D. Hauglustaine, I. Isaksen, J. Lelieveld, D.H. Lister, R. Sausen, U. Schumann, A. Wahner, P. Wiesen, European scientific assessment of the atmospheric effects of aircraft emissions, Atmos. Env. 32 (1998) 2329–2418.

[8] R.C. Brown, R.C. Miake-Lye, C.E. Kolb, A.A. Sorokin, Ya.Y. Buriko, Aircraft exhaust sulfur emissions, Geophys. Res. Lett. 23 (1996) 3603–3606.

[9] R.C. Brown, R.C. Miake-Lye, M.R. Anderson, C.E. Kolb, Effect of aircraft exhaust sulfur emission on near field plume aerosols, Geophys. Res. Lett. 23 (1996) 3607–3610.

[10] H.F. Calcote, Ionic mechanisms of soot formation, in: J. Lahaye, G. Prado (Eds.), Soot in combustion systems and its toxic properties, NATO Conference series. Series VI: Materials Science, Plenum Press, New York, 1981, pp. 197–215.

[11] H.F. Calcote, D.G. Keil, The role of ions in soot formation, Pure Appl. Chem. 62 (1990) 815–824.

[12] G.G. Chernyi, S.A. Losev (Eds.), Physical and chemical processes in gas dynamics. V. 1. Cross sections and rate constants for physical and chemical processes (2002), in press.

[13] J. Curtius, B. Sierau, F. Arnold, R. Baumann, R. Busen, P. Schulte, U. Schumann, First sulfuric acid detection in the exhaust plume of a jet aircraft in flight, Geophys. Res. Lett. 25 (1998) 923–926.

[14] J. Curtius, F. Arnold, P. Schulte, Sulfuric acid measurements in the exhaust plume of a jet aircraft in flight: Implications for the sulfuric acid formation efficiency, Geophys. Res. Lett. (2002), in press.

[15] N.G. Dautov, A.M. Starik, On the problem of choosing a kinetic scheme for the homogeneous reaction of methane with air, Kinetics and Catalysis 38 (1997) 185–208.

[16] W.B. DeMore, S.P. Sander, D.M. Golden, R.F. Hampson, M.J. Kurylo, C.J. Howard, A.R. Ravishankara, C.E. Kolb, M.J. Molina, Chemical kinetics and photochemical data for use in stratospheric modeling. Evaluation 11, JPL Publication 94-26. Jet propulsion laboratory, Pasadena, California (1994).

[17] A.N. Eraslan, R.C. Brown, Chemiionization and ion–molecule reactions in fuel-rich acetylene flames, Combust. Flame 74 (1988) 19–37.

[18] D.W. Fahey et al., Emission measurements of the Concorde supersonic aircraft in the lower stratosphere, Science 270 (1995) 70–74.

[19] F.C. Fehsenfeld, C.J. Howard, A.L. Schmeltekopp, Gas phase ion chemistry of HNO_3, J. Chem. Phys. 63 (1975) 2835–2841.

[20] F.C. Fehsenfeld, I. Dotan, D.J. Albritton, C.J. Howard, E.E. Ferguson, Stratospheric positive ion chemistry of formaldehyde and methanol, J. Geophys. Res. 83 (1978) 1333–1336.

[21] E.E. Ferguson, Negative ion-molecular reactions, Canadian J. Chem. 47 (1969) 1815–1820.

[22] A.B. Fialkov, Investigations on ions in flames, Progr. Energy Comb. Sci. 23 (1997) 399–528.

[23] A. Frenzel, F. Arnold, Sulfuric acid cluster ion formation by jet engines: Implications for sulfuric acid formation and nucleation. DLR-Mitt. 94-06, Deutsches Zentrum für Luft- und Raumfahrt, Köln, Germany (1994) 106–112.

[24] J. Goodings, K.D. Bohme, T.M. Sugden, Sixteenth Symposium (International) on Combustion, The Combustion Institute, Pittsburgh, 1977, pp. 891–902.

[25] J.F. Griffits, J.A. Barnard, Flame and Combustion, Chapman and Hall, London, 1995.

[26] R.W.F. Gross, J.F. Bott (Eds.), Handbook of Chemical Lasers. A Wiley-Interscience Publication, John Wiley and Sons, New York, 1976.

[27] J.E. Penner, D.H. Lister, D.J. Griggs, D.J. Dokken, M. McFarland (Eds.), Aviation and the Global Atmosphere, A Special Report of IPCC (Intergovernmental Panel on Climate Change), Cambridge Univ. Press, Cambridge, UK, 1999.

[28] B. Kärcher, F. Yu, F.P. Schröder, R.P. Turco, Ultrafine aerosol particles in aircraft plumes: Analysis of growth mechanisms, Geophys. Res. Lett. 25 (1998) 2793–2796.

[29] B. Kärcher, R.P. Turco, F. Yu, M.Y. Danilin, D.K. Weisenstein, R.C. Miake-Lye, R. Busen, On the unification of aircraft ultrafine particle emission data, J. Geophys. Res. 105 (2000) 29379–29386.

[30] H. Kawamoto, T. Ogawa, Steady state model of negative ions in the lower atmosphere, Planetary and Space Science 32 (1984) 1223–1233.

[31] D.G. Keil, R.J. Gill, D.B. Olson, F. Calcote, Ion concentrations in premixed acetylene-oxygen flames near the soot threshold, in: T.M. Sloane (Ed.), The Chemistry of Combustion Processes, ACS Symposium Series, Vol. 249, American Chemical Society, Washington, 1984, pp. 33–47.

[32] A. Kiendler, S. Aberle, F. Arnold, Negative chemiions formed in jet fuel combustion: New insights from jet engine and laboratory measurements using a quadrupole ion trap mass spectrometer apparatus, Atmos. Env. 34 (2000) 2623–2632.

[33] A. Kiendler, S. Aberle, F. Arnold, Positive ion chemistry in the exhaust plumes of an aircraft jet engine and a burner: Investigations with a quadrupole ion trap mass spectrometer, Atmos. Env. 34 (2000) 4787–4793.

[34] O. Knab, T.A. Gogel, H.-H. Frühauf, E.W. Messerschmid CVCV-model validation by means of radiative heating calculations, AIAA 95-0623 (1995).

[35] I.A. Kossyi, Yu.A. Kostinsky, A.A. Matveyev, V.P. Silakov, Kinetic scheme of the non-equilibrium discharge in nitrogen–oxygen mixtures, Plasma Sources Sci. Techn. 1 (1992) 207–220.

[36] S.P. Lukachko, I.A. Waitz, R.C. Miake-Lye, R.C. Brown, M.R. Anderson, Production of sulfate aerosol precursors in the turbine and exhaust nozzle of an aircraft engine, J. Geophys. Res. 103 (1998) 16159–16174.

[37] V.N. Makarov, Construction of the optimal kinetic models in physical-chemical gas dynamics, Dissertation of Doctor of Science in Physics and Mathematics, Moscow State University (1996).

[38] R.C. Miake-Lye, B.E. Anderson, W.R. Cofer, H.A. Wallio, G.D. Nowicki, J.O. Ballenthin, D.E. Hunton, W.B. Knighton, T.M. Miller, J.V. Seeley, A.A. Viggiano, SO_x oxidation and volatile aerosol in aircraft exhaust plumes depend on fuel sulfur content, Geophys. Res. Lett. 25 (1998) 1677–1680.

[39] R.C. Miake-Lye, A.T. Chobot, S.P. Lukachko, R.C. Brown, J. Zhang, I.A. Waitz, Simulation of post-combustion chemical evolution in gas turbine engines, in: U. Schumann, G.T. Amanatidis (Eds.), Aviation, Aerosols, Contrails and Cirrus Clouds, 2001, pp. 95–98. EUR 19428, European Commission, Brussels.

[40] C. Park, Nonequilibrium Hypersonic Aerothermodynamics, Wiley, New York, 1990.

[41] T. Pedersen, R.C. Brown, Simulation of electric field effects in premixed methane flames, Combust. Flame 94 (1993) 433–448.

[42] J.C. Person, D.O. Ham, Removal of SO_2 and NO_x from stack gases by electron beam irradiation, Radiative Physical Chemistry 31 (1988) 1–8.

[43] J. Peters, G. Mahnen, Fourteenth Symposium (International) on Combustion, The Combustion Institute, Pittsburgh, 1972, 133–146.

[44] B.V. Potapkin, V.D. Rusanov, M.I. Strelkova, A.A. Fridmann, Investigation of kinetics and energetics of dissociation processes of H_2S mixed with CO_2 in thermal plasma, High Energy Chemistry 23 (1992) 63–68.

[45] T. Reiner, F. Arnold, Laboratory flow reactor measurements of the reaction $SO_3 + H_2O + M \rightarrow H_2SO_4 + M$: Implications for gaseous H_2SO_4 and aerosol formation in the plume of jet aircraft, Geophys. Res. Lett. 20 (1993) 2659–2662.

[46] A.M. Savel'ev, A.M. Starik, N.S. Titova, Investigation of the dynamics of formation of environmentally harmful gases in elements of gas turbine engine, High Temperature 37 (1999) 470–478.

[47] O.P. Schatalov, in: G.G. Cherniy, V.A. Levin (Eds.), Nonequilibrium Gas Flow with Physico-Chemical Transformation, Moscow State University, 1980, pp. 39–62.

[48] P. Schulte, H. Schlager, H. Ziereis, U. Schumann, S.L. Baughcum, F. Deidewig, NO_x emission indices of subsonic long-range jet aircraft at cruise altitude: In situ measurements and predictions, J. Geophys. Res. 102 (1997) 21431–21442.

[49] U. Schumann (Ed.), AERONOX – The impact of NO_x emissions from aircraft upon the atmosphere at flight altitudes 8–15 km. EUR 16209, 1995, 471 pp. Office for Publications of the European Community, Brussels.

[50] U. Schumann, J. Ström, R. Busen, R. Baumann, K. Gierens, M. Krautstrunk, F.P. Schröder, J. Stingl, In situ observations of particles in jet aircraft exhausts and contrails for different sulfur containing fuels, J. Geophys. Res. 101 (1996) 6853–6899.

[51] U. Schumann, H. Schlager, F. Arnold, R. Baumann, P. Haschberger, O. Klemm, Dilution of aircraft exhaust plumes at cruise altitudes, Atmos. Env. 32 (1998) 3097–3103.

[52] U. Schumann, H. Schlager, F. Arnold, J. Ovarlez, H. Kelder, Ø. Hov, G. Hayman, I.S.A. Isaksen, J. Staehelin, P.D. Whitefield, Pollution from aircraft emissions in the North Atlantic flight corridor: Overview on the POLINAT projects, J. Geophys. Res. 105 (2000) 3605–3631.

[53] U. Schumann, F. Arnold, R. Busen, J. Curtius, B. Kärcher, A. Kiendler, A. Petzold, H. Schlager, F. Schröder, K.-H. Wohlfrom, Influence of fuel sulfur on the composition of aircraft exhaust plumes: The experiments SULFUR 1-7, J. Geophys. Res. 107 (2002), in press.

[54] J.V. Seeley, R.A. Morris, A.A. Viggiano, Rate constants for the reactions of $CO_3^-(H_2O)_{n=0-5} + SO_2$: implications for CIMS detection of SO_2, Geophys. Res. Lett. 24 (1997) 1379–1382.

[55] K. Smith, R.M. Thompson, Computer Modeling of Gas Lasers, Plenum Press, New York, 1978.

[56] A.M. Starik, N.S. Titova, L.S. Yanovskii, Analysis of the singularities of the kinetics of combustion of the products of thermal destruction of n-octane mixed with air, High Temperature 37 (1999) 270–281.

[57] A.M. Starik, N.S. Titova, L.S. Yanovskii, Kinetics of the oxidation of the products from the thermal destruction of C_3H_8 and n-C_4H_{10} in the mixtures with air, Kinetics and Catalysis 40 (1999) 7–22.

[58] H.G. Tremmel, U. Schumann, Model simulations of fuel sulfur conversion efficiencies in an aircraft engine: Dependence on reaction rate constants and initial species mixing ratios, Aerosp. Sci. Technol. 3 (1999) 417–430.

[59] H.G. Tremmel, H. Schlager, P. Konopka, P. Schulte, F. Arnold, M. Klemm, B. Droste-Franke, Observations and model calculations of jet aircraft exhaust products at cruise altitude and inferred initial OH emissions, J. Geophys. Res. 103 (1998) 10803–10816.

[60] F. Yin, D. Grosjean, J.H. Seinfeld, Analysis of atmospheric photooxidation mechanism for organosulfur compounds, J. Geophys. Res. 91 (1986) 14417–14438.

[61] F. Yu, R.P. Turco, The role of ions in the formation and evolution of particles in aircraft plumes, Geophys. Res. Lett. 24 (1997) 1927–1930.

[62] F. Yu, R.P. Turco, B. Kärcher, F.P. Schröder, On the mechanisms controlling the formation and properties of volatile particles in aircraft wakes, Geophys. Res. Lett. 25 (1998) 3839–3842.